Fatigue reliability of mooring chains, including mean load and corrosion effects

Erling N. Lone[a,*], Thomas Sauder[b,a], Kjell Larsen[a,c], Bernt J. Leira[a]

[a]*Department of Marine Technology, Norwegian University of Science and Technology, Trondheim N-7491, Norway*
[b]*SINTEF Ocean, P.O. Box 4762 Torgarden, 7465 Trondheim, Norway*
[c]*Equinor ASA, Arkitekt Ebbells veg 10, 7053 Ranheim, Norway*

Abstract

A reliability formulation for mooring chain fatigue is developed based on the S–N approach. The effects of mean load and degradation due to corrosion are included by starting from a S-N model with parameterized dependence to the mean load and a customized corrosion condition scale. Partial dependence between the failure events of individual links within a chain segment is addressed by distinguishing between properties and loads that are assumed to be either independent or fully correlated between links. The paper includes a thorough case study, based on a realistic case. A global sensitivity analysis is presented, to assess the importance of interaction between random variables and to justify a reduction of the model dimension. A reliability analysis is then performed, and the effect on failure probability from variation of a range of parameters and model assumptions is studied.

Keywords: Studless chain, S-N approach, Sensitivity analysis, Reliability analysis, Mean load, Corrosion

1. Introduction

Fatigue assessment of offshore mooring systems is required by relevant rules and standards [1, 2], to demonstrate satisfactory resistance towards exposure to cyclic loads. These fatigue calculations are subject to considerable uncertainties with respect to both loads and capacity, requiring fatigue safety factors typically ranging from 5 to 8 [2]. These fairly large safety factors aim to satisfy a maximum annual probability of mooring line failure in the range from 10^{-3} to 10^{-5} [2–4]. Nevertheless, mooring lines historically tend to fail at a much higher rate [5–7]. The root causes are diverse, however; almost half of the events described in [7] were related to chain components and almost half of those were caused by fatigue and corrosion. Likely contributors to these failures are uncertainties in dynamic loads and a lack of proper models to account for effects governing the fatigue capacity of mooring chains.

*Corresponding author.
Email addresses: erling.lone@ntnu.no (Erling N. Lone), thomas.sauder@sintef.no (Thomas Sauder), kjell.larsen@ntnu.no (Kjell Larsen), bernt.leira@ntnu.no (Bernt J. Leira)

The fatigue capacity curves prescribed by current design codes [1, 2] are based on fatigue tests of new chain performed at a mean load of 20% of the minimum breaking load (MBL) [8]. In the fatigue calculations, the actual mean loads of the mooring lines are disregarded, whereas degradation due to corrosion is accounted for in a simplified manner by reducing the cross section area of the chains, giving an increase in the effective stress ranges entering the calculations. However; full scale fatigue tests performed in recent years for both new and used studless mooring chains have revealed that (i) the fatigue capacity of chains is strongly dependent on the mean load, and (ii) realistic corrosion pits have a detrimental effect not well represented by the simplified approach prescribed by the standards [8–12]. Hence, proper treatment of mean load effect and degradation due to corrosion in the calculations seems imperative to enable improved estimation of mooring line fatigue life.

Based on test results for new and used chain, tested at a range of mean load levels and with various degrees of corrosion, Lone et al. [12] established a fatigue capacity model with parameterized dependence to mean load and a customized corrosion measure. This work formed the basis for a probabilistic fatigue damage model, presented in [13]. In the present paper, we further develop the probabilistic model into a formulation of fatigue reliability for mooring chain segments that for the first time accounts properly for mean load and corrosion effects. We herewith provide the necessary basis for enabling a reliability-based integrity management of mooring chain fatigue (illustrated in Figure 1). This is the main contribution of the paper. However, it is written in a more comprehensive way, for accessibility to readers with main background in mooring line engineering and to a lesser extent in reliability methods.

The paper is organized as follows. In Section 2, we review the mean load and corrosion dependent fatigue capacity model and the probabilistic fatigue damage model. In Section 3, we develop the reliability formulation for fatigue failure of mooring chain segments, and discuss the need for extension into considering entire mooring lines as well as some relevant aspects of the reliability model. In Section 4, we apply the reliability formulation to a case study to discuss relevant assumptions and properties of the fatigue reliability model. Conclusions are given in Section 5.

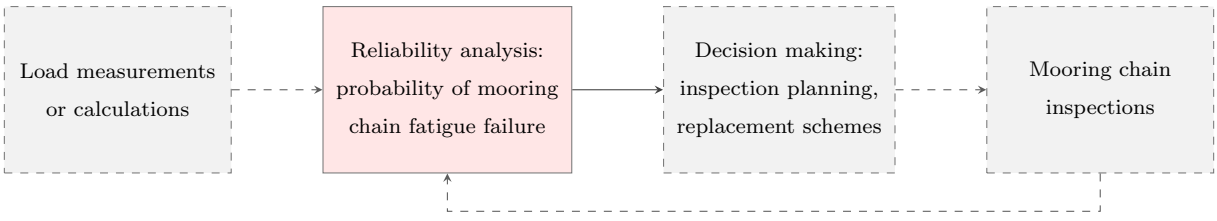

Figure 1: Simplified illustration of reliability-based integrity management of mooring chain fatigue. The scope of the present study is indicated by the red box with solid border.

2. Probabilistic fatigue model

In this section, we review the mean load and corrosion dependent fatigue capacity model and the probabilistic fatigue damage model in the context of the present paper. We apply the usual convention of describing random variables by capital letters (e.g., X), small letters to describe a realization of a random variable (e.g., x), and bold symbols to denote vectors or matrices (e.g., $\boldsymbol{X}, \boldsymbol{x}$).

2.1. Mean load and corrosion dependent fatigue capacity

The S-N approach to fatigue of mooring chain is considered. Fatigue capacity is then expressed in terms of a stress-life (S-N) curve, defined as

$$N \cdot S^m = A \tag{1}$$

where N is the number of cycles to failure at constant stress range S, m is the slope parameter and A is referred to as the intercept parameter. To account for the effect of mean load and corrosion on the fatigue capacity, Lone et al. [12] expressed the intercept parameter as function of these parameters:

$$\log A(\sigma_m, c) = B_0 + B_1 \cdot g_1(\sigma_m) + B_2 \cdot g_2(c) \tag{2}$$

where $\log(.)$ is the common logarithm, $(B_j)_{j\in\{0,1,2\}}$ are coefficients and $g_1(\sigma_m)$ and $g_2(c)$ are monotonically increasing functions of the mean stress (σ_m) and a corrosion grade (c), respectively. The corrosion grade applied here is based on a customized scale ranging from 1 (new chain or mild corrosion) to 7 (severe corrosion), see [12] for details.

Equations (1) and (2) constitute a mean load and corrosion dependent S-N model as follows. For a given stress range effect (m), the fatigue capacity (or number of cycles to failure) is proportional to the intercept parameter, A. The first term in (2) describes the constant (time-invariant) part of the fatigue capacity. The second term describes the mean load effect; a negative value of B_1 implies that the fatigue capacity increases when the mean load is reduced. The last term describes the deteriorating effect of corrosion; a negative value of B_2 implies that the fatigue capacity is reduced when the corrosion grade increases.

The coefficients of the mean load and corrosion dependent S-N model were estimated empirically from a database of full scale fatigue tests, by considering the following regression model

$$\begin{aligned} \log N_i &= B_0 + B_1 \cdot g_1(\sigma_{m,i}) + B_2 \cdot g_2(c_i) - m \cdot \log S_i + \epsilon_i \\ \epsilon_i &\sim N(0, \sigma_\epsilon^2) \end{aligned} \tag{3}$$

with the stress range effect fixed at $m = 3$. Here, the subscript i is a counter for fatigue test samples and ϵ is the regression error representing the predictive uncertainty of the regression model, see e.g., [14].

In total the database consisted of 125 samples of studless chain, tested at various mean loads and for various degrees of corrosion; 77 tests for used chains retrieved after operation in the North Sea, and 48 tests

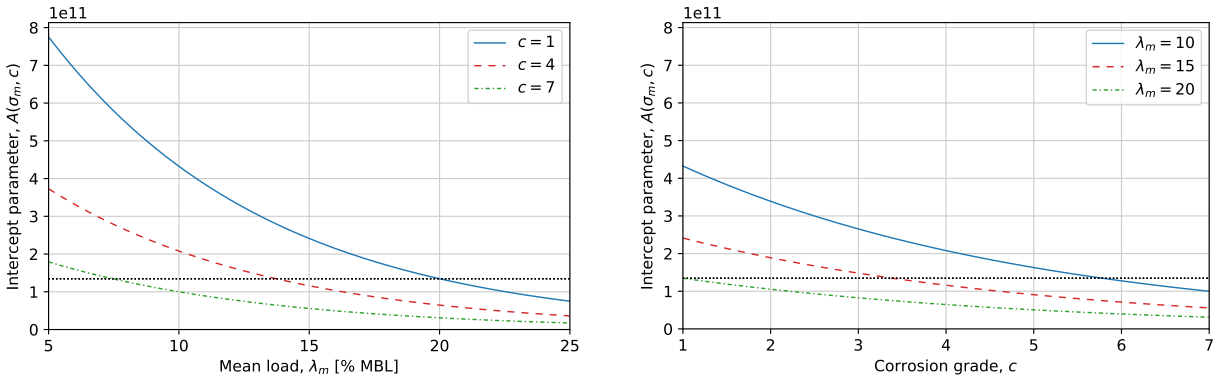

Figure 2: S-N curve intercept parameter fitted to fatigue tests of used and new chains [12], as function of mean load (left) and corrosion grade (right). The horizontal dotted line is located at a reference value $A = 1.346 \times 10^{11}$ ($\log A = 11.129$) corresponding to $\lambda_m = 20$ [% MBL] and $c = 1$.

for new chains. Different functional relationships to the mean load and corrosion grade were assessed, and the most adequate mean load function was found to be $g_2(\sigma_m) = \lambda_m$, where λ_m is the mean load expressed in percentage of the minimum breaking load (MBL). For corrosion grade, the best fit to data was achieved with $g_2(c) = c$. S-N model parameters obtained from least-squares regression in [12] are listed in Table 1, and the corresponding intercept parameter is visualized in Figure 2 for various values of the mean load and corrosion grade.

Table 1: S-N curve parameters estimated by least-squares regression with $m = 3$, from fatigue tests of used and new studless chains [12].

$g_1(\sigma_m)$	$g_2(c)$	$\hat{B}_0$	$\hat{B}_1$	$\hat{B}_2$	$\hat{\sigma}_\epsilon$
λ_m	c	12.249	-0.0507	-0.106	0.17

This S-N model forms the basis for the probabilistic fatigue damage model described in the next subsection. Note that although we have presented the preferred functional relationships between the intercept and mean load and corrosion grade, we will retain the generic notation $g_1(.)$ and $g_2(.)$ in the subsequent section for the sake of generality.

2.2. Probabilistic fatigue damage

We now introduce the following assumptions:

- The Palmgren-Miner hypothesis on linear accumulation of the fatigue effect from each stress cycle is adopted for variable amplitude loading.
- The S-N curve slope parameter (stress range effect, m) is assumed fixed.
- Time-variant random variables may be considered as piecewise time-invariant.

Furthermore, we introduce a *fatigue load* variable as

$$Z = n_0 \cdot \mathrm{E}[S^m] \tag{4}$$

where n_0 is the number of stress cycles and $\mathrm{E}[S^m]$ is the m^{th} moment of the stress range distribution for a given time period. By application of Miner's rule, the fatigue damage after N_y years may then be expressed as a summation over annual contributions [13]:

$$D(\boldsymbol{X}; N_y) = \sum_{k=1}^{N_y} \frac{Z_k}{10^{\left(B_0 + B_1 \cdot G^*_{1,k} + B_2 \cdot G^*_{2,k} + \epsilon\right)}} \tag{5}$$

where $\boldsymbol{X} = (B_0, B_1, B_2, \epsilon, \boldsymbol{Z}, \boldsymbol{G}^*_1, \boldsymbol{G}^*_2)$ is a vector of the underlying random variables, k is a counter for years, and $G^*_{1,k}$ and $G^*_{2,k}$ are representative values of the mean load and the corrosion grade functions in the k^{th} year, respectively. Note that in [13], the uncertainty associated with the S-N model error (ϵ) was included in the uncertainty of B_0. Here, we choose to express this uncertainty explicitly, for reasons that will become clear in Section 3. Also note that, when expressed as a function of the random vector $\boldsymbol{X}$, the fatigue damage in (5) is stochastic quantity. In the following, we will describe (5) and define the elements of $\boldsymbol{X}$ that were not covered by the description of the S-N model in the previous subsection, namely $\boldsymbol{Z}$, $\boldsymbol{G^*_1}$ and $\boldsymbol{G^*_2}$.

This fatigue damage model enables accounting for both prior, known loads and future, uncertain loads. Hence, the vector $\boldsymbol{Z}$, containing fatigue loads for each of the N_y years, may consist of both deterministic and random quantities. For instance; if the damage is estimated for N_p prior years and N_f future years, we have $\boldsymbol{Z} = (z_1, \ldots, z_{N_p}, Z_{N_y - N_f + 1}, \ldots, Z_{N_y})$. That is, $\boldsymbol{Z}$ then consists of N_p deterministic quantities and N_f random quantities.

The mean load and corrosion dependent intercept parameter in (2) introduces a time-dependency to the fatigue capacity, which varies both over years and during the course of each year due to mean load variations and the temporal corrosion development. The annual variations are accounted for by allowing the values of G^*_1 and G^*_2 to vary by year in Equation (5). By introducing representative values for the mean load and corrosion grade functions, we ensure that the piecewise time-invariant summation accounts properly also for the within-year variations.

The vector of representative mean load values ($\boldsymbol{G^*_1}$) is constructed in a way similar to that of the fatigue loads. For the N_p prior years with known load history, the representative mean load values are calculated deterministically from the joint, empirical distributions of mean loads and stress ranges for each year [13]:

$$g^*_{1,k} = -\frac{1}{b_1} \log \left[\frac{\sum_i n_i \cdot s_i^m \cdot 10^{-b_1 \cdot g_1(\sigma_{m,i})}}{n_{0,k} \cdot \mathrm{E}[S^m]_k} \right] \tag{6}$$

where index i refers to tuples with $(n_i, s_i, \sigma_{m,i})$ from a joint histogram of stress ranges and mean stress: n_i is the number of joint occurrences of stress range s_i and mean stress $\sigma_{m,i}$, $n_{0,k} = \sum_i n_i$ is the total number of stress cycles, $\mathrm{E}[S^m]_k = \frac{1}{n_{0,k}} \sum_i n_i \cdot s_i^m$ is the m^{th} moment of the stress range distribution, and

all summations are over observations in the k^{th} year. In this calculation, the mean load coefficient B_1 is assumed fixed at a given value b_1. However, as demonstrated by the following example, the representative mean load calculated from (6) is typically insensitive to variations in the mean load coefficient.

Example 1. We consider the hindcast-based simulations presented in [13] for the mooring system of a typical semi-submersible production unit in the Norwegian Sea.[1] The representative mean load is calculated for the years 2001-2010 using Equation (6) with the mean load function $g_1(\sigma_m) = \lambda_m$ [% MBL] with three different values of b_1: the estimated value from regression analysis, $\hat{B}_1 = -0.0507$ (Table 1), and $\hat{B}_1 \pm 2 \cdot \hat{\sigma}_{B_1}$ where $\hat{\sigma}_{B_1} = 0.0045$ is the estimated standard error of $\hat{B}_1$ [13, Sec. 4]. The resulting values for g_1^* are presented in Figure 3, showing negligible difference for the lower and upper values of the estimated representative mean load for each year. Hence, for the S-N model in Table 1 and the mooring line considered in the current example, a fixed value of B_1 may be used for the calculation of representative mean load, regardless of whether a fixed or stochastic mean load coefficient is assumed for the probabilistic analysis.

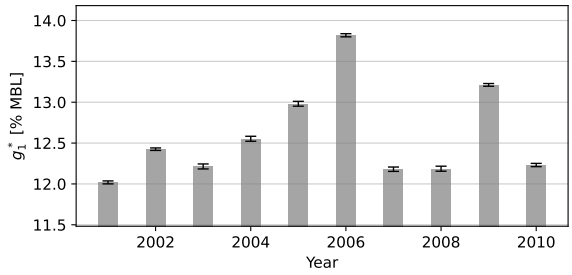

Figure 3: Example of annual representative mean loads for a semi-submersible in the Norwegian Sea, calculated for $b_1 = \hat{B}_1$ (bars) and $b_1 = \hat{B}_1 \pm 2 \cdot \hat{\sigma}_{B_1}$ (error bars). The limits of the vertical axis have been narrowed down to make the upper and lower values of the error bars distinguishable.

For the N_f future years, the representative mean load is generally represented by stochastic quantities. A fixed value for future years may however be justified if the annual variability is found to be sufficiently low, or if the effect of annual variability on the quantity of interest is shown to be negligible. Note that results presented in [13] showed that the representative mean load may be correlated with the annual fatigue load. Alternative ways to address this correlation are discussed in Section 3.

For the corrosion grade function, $\boldsymbol{G_2^*}$ is a tuple containing the representative value for each of the N_y years, implicitly describing the corrosion grade development and the corresponding chain degradation. However, unlike the fatigue load and representative mean load, the corrosion grade may be subject to uncertainty for both prior and future years. This may be the case even if inspections are performed, since the categorization from inspection will itself be subject to some uncertainty. Furthermore, inspections are discrete events and

[1] The current calculations are performed for mooring line 1 of the system considered, see [13, Sec. 3] for details.

will therefore yield corrosion grade estimates for those specific points in time, but not for the intermediate time periods. Hence, in the case of chain inspections, the construction of $\boldsymbol{G_2^*}$ must be based on an assessment of the quality and uncertainty of the inspections, as well as the uncertainty of the intermediate and future states. On the other hand, if nothing is known about the corrosion state of the chains it may be convenient to let $\boldsymbol{G_2^*}$ be a function of some underlying random variable(s), such as for instance the corrosion grade at the end of the service life and some parameter that describes the shape of its temporal development. This is illustrated in the following example.

Example 2. Consider the corrosion grade function $g_2(c) = c$, and the following model for the corrosion grade development [13]:

$$C_k = 1 + (C_{\text{end}} - 1) \cdot (\frac{k-a}{L})^{\eta} \tag{7}$$

where $L \in \mathbb{N}^*$ is the service life, $k \in \{1, \ldots, L\}$ is a counter for year, C_{end} is a random variable representing the corrosion grade at the end of the service life, η is an exponent that determines the shape of the time history, and $a \in [0, 1]$ controls which value is taken as the representative one. For example, $a = 0.5$ implies that the corrosion grade is represented by its value halfway through that year, whereas $a = 0$ means that the value at the end of the year is used. A reasonable choice for the representative corrosion grade function would then be $G^*_{2,k} = C_k$, which gives $\boldsymbol{G_2^*} = (C_1, ..., C_{N_y})$. Hence, assuming that the parameters (a, L, η) are fixed, the vector $\boldsymbol{G_2^*}$ is a function of the random variable C_{end} only. Examples of corrosion grade histories for different shape parameters are shown in Figure 4.

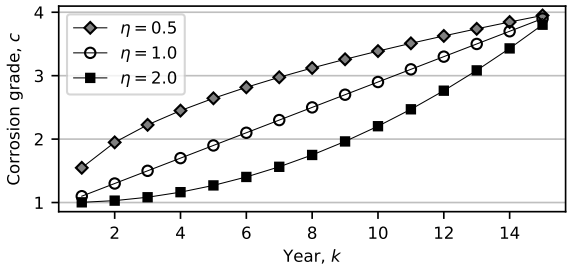

Figure 4: Examples of corrosion grade histories calculated from Equation (7) with $C_{\text{end}} = 4$, $L = 15$, $a = 0.5$ and different shape parameters.

In summary, the fatigue damage model in Equation (5) represents an adaption of Miner's rule for damage accumulation that enables accounting for (i) the annual fatigue load variability, (ii) the effect on fatigue capacity from mean load (including time dependent variations) and degradation due to corrosion, and (iii) possible interactions between these. This forms the basis for the mooring chain reliability formulation that is developed in the next section.

3. Reliability formulation

In this section, we first define the failure criterion for a *single* chain link. This is thereafter used as a starting point for developing the reliability formulation for a chain *segment*. We proceed by defining limit state functions for link and segment failure, and discuss various aspects of the probabilistic model.

3.1. Failure of single link

For a deterministic case, fatigue failure is assumed to occur when the fatigue damage reaches unity. The corresponding failure criterion is then $D \geq 1$. In practice, Miner's rule is imperfect and subject to considerable uncertainty. Wirsching [15] therefore argued that a more appropriate failure criterion is $D \geq D_{\text{cr}}$, where $D_{\text{cr}} \in \mathbb{R}_+$ is a random variable denoting the "critical" damage (i.e., the Miner's sum at failure). The probability of failure for a single chain link may then be expressed as

$$p_f^{(1)} = \mathrm{P}\left[D_{\text{cr}} \leq D(\boldsymbol{X}; N_y)\right] \tag{8}$$

where superscript $\cdot^{(1)}$ indicates that the failure event is for *one* link.

3.2. Failure of chain segment

A chain *segment* is here defined as a continuous mooring line section, composed of identical chain links. As such, it constitutes a classical series system where failure of a single component (here: chain link) leads to system (segment) failure. Unfortunately, the formulation in (8) is inappropriate for direct calculation of segment failure probability in the presence of partial correlation between the failure events of the links. As illustrated by the following example, segment failure probability may be considerably over- or underestimated if partial dependence between the individual links is ignored or mistreated.

Example 3. Consider a mooring chain segment composed of N identical links, and let the probability of failure in any one of these links be identical and equal to $p_f^{(1)}$. Two limiting cases may then be defined for the failure probability for this segment: (i) the failure events for each of the links are *fully correlated*, or (ii) the failure events are *mutually independent*. The failure probability for these limiting cases is [see e.g., 16, Chapter 3]:

$$p_f^{(N)} = \begin{cases} p_f^{(1)} & \text{if fully correlated} \\ 1 - \left[1 - p_f^{(1)}\right]^N & \text{if independent} \end{cases} \tag{9}$$

The resulting failure probability is shown as a function of number of components (links) in Figure 5, assuming $p_f^{(1)} = 10^{-6}$. With 100 links, the failure probability is two orders of magnitude higher for the case with independence, and with 1000 links the difference is three orders of magnitude.

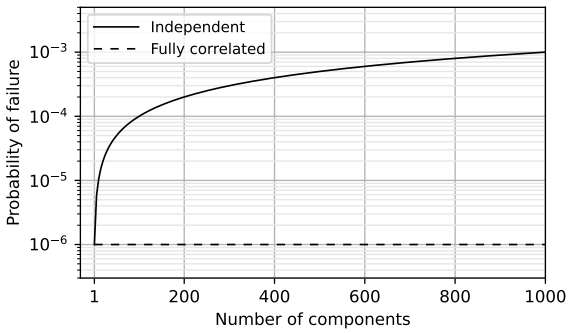

Figure 5: Probability of failure for a series system as function of number of components for the two limiting cases (independent vs. fully correlated failure events), assuming probability of failure in any one component is 10^{-6}.

Instead of considering the failure *events* as either fully correlated or independent, Larsen and Mathisen [17] accounted for the partial correlation by distinguishing between the *variables* that are fully correlated between links and those that may be assumed to be independent. A similar approach is applied here. We assume that the following variables and properties are the *same* between links:

- $\boldsymbol{Z}$ (fatigue loads). This is considered a reasonable and realistic assumption, as links within a chain segment will indeed be exposed to very similar *dynamic* loads (hence, similar stress range distributions). Any deviations in the loads within a segment are assumed to be of minor importance.
- $\boldsymbol{G_1^*}$ (mean loads). Analogously, the mean loads are assumed to be the same for links within a segment. This is a slightly less accurate assumption, since the mean load in a catenary line will generally decrease with increasing distance from the fairlead in direction of the anchor.[2] Nevertheless, the mean loads within a segment will be practically fully correlated, and conservatism may be ensured by using the highest mean load within the segment (that is, typically the mean load for the link closest to the fairlead).
- $\boldsymbol{G_2^*}$ (corrosion grades). Some variation of the corrosion grade would be expected along a segment, depending on segment length, location (position in water column, sea bed contact, etc.) and due to the inherent variability of the corrosion process. The need for a model addressing its spatial variation could therefore be justified. Here, we simplify the problem by assuming that the same corrosion grade applies to the entire segment. Conservatism may then be ensured by considering the most severe corrosion grade along the segment length as representative for all links. In the case that inspections reveal a systematic variation from one end of the segment to the other, this could be addressed by modeling the segment as two or more separate segments with different values for the corrosion grade.
- B_0, B_1, B_2 (S-N model parameters). This implies that the mean load and corrosion grade effects are

[2]There are exceptions to this general rule, for instance in the presence of buoys. However, by definition, chain links on different sides of a buoy would be considered as parts of separate chain segments.

assumed to be the same, and consequently, that the *median* fatigue capacity is the same for each link. This is consistent with the regression model in Equation (3).

- D_{cr} (Miner's sum at failure). According to Lotsberg [18, p. 115], the accuracy of Miner's rule is related to the shape of the fatigue load spectra. Hence, following the above assumption of similar fatigue loads, it is reasonable to assume the same Miner's sum at failure for links within a segment.

On the other hand, we assume that the *deviation* from the median fatigue capacity, expressed in terms of the S-N model error (ϵ), is independent and identically distributed (i.i.d.) for each link. Again, this assumption is consistent with the regression model in Equation (3).

The fatigue damage for the i^{th} component may then be expressed as:

$$D_i(\boldsymbol{X}_i; N_y) = \frac{1}{10^{\epsilon_i}} \sum_{k=1}^{N_y} \frac{Z_k}{10^{\left(B_0 + B_1 \cdot G^*_{1,k} + B_2 \cdot G^*_{2,k}\right)}} \tag{10}$$

where the vector of random variables $\boldsymbol{X}_i$ here contains one independent variable (ϵ_i), whereas the remaining variables take on the same value for all links ($B_0, B_1, B_2, \boldsymbol{Z}, \boldsymbol{G^*_1}, \boldsymbol{G^*_2}$). The corresponding failure probability for the i^{th} component is then:

$$p_f^{(i)} = \text{P}\left[D_{\text{cr}} \leq \frac{1}{10^{\epsilon_i}} \sum_{k=1}^{N_y} \frac{Z_k}{10^{\left(B_0 + B_1 \cdot G^*_{1,k} + B_2 \cdot G^*_{2,k}\right)}} \right] \tag{11}$$

We now define two auxiliary variables that will be useful in the following:

$$R := 10^{\epsilon} \tag{12}$$

$$V(\boldsymbol{X}; N_y) := \frac{1}{D_{\text{cr}}} \sum_{k=1}^{N_y} \frac{Z_k}{10^{\left(B_0 + B_1 \cdot G^*_{1,k} + B_2 \cdot G^*_{2,k}\right)}} \tag{13}$$

For notational convenience, the variable D_{cr} is here appended to the vector of fully dependent random variables, $\boldsymbol{X}$. By utilizing that R and D_{cr} are always positive, Equation (11) may be reorganized into

$$p_f^{(i)} = \text{P}\left[R_i \leq V(\boldsymbol{X}; N_y) \right] \tag{14}$$

This expression has the form of a classical load-resistance formulation for a series system exposed to a common "load" V and with i.i.d. "resistance" R_i. The probability of segment failure may be expressed by means of the event that any of the N links fails or, equivalently, as the complement of the event that all the components survive:

$$p_f^{(N)} = \text{P}\left[\bigcup_{i=1}^{N} (R_i \leq V(\boldsymbol{X}; N_y)) \right] = 1 - \text{P}\left[\bigcap_{i=1}^{N} (R_i > V(\boldsymbol{X}; N_y)) \right] \tag{15}$$

By conditioning on a realization of the variables that are fully correlated between links, $v = V(\boldsymbol{x})$, the failure (or survival) events become statistically independent. Recalling that the R_i are i.i.d., the conditional

probability of segment failure is then

$$p_{f|\boldsymbol{X}=\boldsymbol{x}}^{(N)} = 1 - \prod_{i=1}^{N} \mathrm{P}\left[R_i > v\right] = 1 - \mathrm{P}\left[R > v\right]^N = 1 - \left[1 - F_R(v)\right]^N \tag{16}$$

where $F_R(v) = \mathrm{P}\left[R \leq v\right]$ is the cumulative distribution function (CDF) of R for any single link, evaluated at v. From order statistics, the resulting expression is recognized as the exact distribution of the extreme minimum value of N i.i.d. variables R, see e.g., [19]. In other words, Equation (16) describes an intuitive result; when the "load" (here: v) is the same for all components, segment failure is controlled by the resistance of the weakest link.

Now, let

$$W := \min\left\{R_1, \ldots, R_N\right\} \tag{17}$$

denote the deviation from median fatigue capacity for the weakest out of N chain links, and let $F_W(.)$ denote its CDF. The conditional segment failure probability may then be expressed in a more compact form as

$$p_{f|\boldsymbol{X}=\boldsymbol{x}}^{(N)} = F_W(v; N) \tag{18}$$

The marginal segment failure probability is obtained from the total probability theorem:

$$p_f^{(N)} = \int_{\boldsymbol{X}} F_W(V(\boldsymbol{x}); N)\, f_{\boldsymbol{X}}(\boldsymbol{x})\, \mathrm{d}\boldsymbol{x} \tag{19}$$

where $f_{\boldsymbol{X}}(.)$ is the joint probability density function for $\boldsymbol{X}$. This resulting integral is equivalent to the probability statement [see e.g., 20, Ch. 3]

$$p_f^{(N)} = \mathrm{P}\left[W \leq V\right] \tag{20}$$

which gives an intuitive representation, stating that segment failure is the event that the weakest link "resistance" is less than or equal to the random "load" V. By defining the *weakest link fatigue damage* as

$$D_W(\boldsymbol{X}; N_y, N) := \frac{1}{W} \sum_{k=1}^{N_y} \frac{Z_k}{10^{\left(B_0 + B_1 \cdot G_{1,k}^* + B_2 \cdot G_{2,k}^*\right)}} \tag{21}$$

where W is defined in (17), we may reorganize (20) into

$$p_f^{(N)} = \mathrm{P}\left[D_{\mathrm{cr}} \leq D_W(\boldsymbol{X}; N_y, N)\right] \tag{22}$$

which expresses the probability of segment failure on the same format as that describing single link failure in Equation (8).

3.3. Model uncertainties

Model uncertainties are included in probabilistic models to account for the uncertainties and possible bias in the mathematical models representing physical effects, and the inaccuracies in the underlying data

used to define the input to the calculations. Relevant examples include the use of a S-N model and Miner's rule to represent the fatigue effect, and inaccuracies in load measurements or in numerical models used for response simulations. In fact, we have already included one model uncertainty by introducing the random variable D_{cr} to represent the Miner's sum at failure (cf. Section 3.1). Here, we introduce additional random variables to account for inaccuracies in stress ranges, mean loads and corrosion grade.

Stress ranges. Estimated stress ranges normally originate from one of the following sources: (i) mooring line tension measurements, (ii) mooring system response calculations or (iii) a combination of these. In the former case, measurement errors cause inaccuracies that will depend on for instance sensor type, time since last calibration and frequency resolution. In the case of response calculations, stress range errors arise from for instance inaccuracies in the numerical models (e.g., mooring component properties and environmental load coefficients for the floater), assumptions about operational parameters (e.g., draft and heading of floater, mooring line pretension) and the modeling of environmental loads (wind, waves and current). In general, the magnitude of the respective errors may be reduced by increasing the estimation effort, for instance by improved sensors or measurement techniques, by use of model tests for calibration of numerical models [21, 22] or by combining measurements and response calculations in a sensible way. The errors may, however, never be completely eliminated. For all cases, we assume that the *true* stress range may be quantified as $S' = Q_s \cdot S$, where Q_s is a random variable denoting stress range error and S is the estimated stress range. Assuming that Q_s is time-invariant and independent of the estimated stress range, the true fatigue load may then be expressed as

$$Z' = n_0 \int_S (Q_s \cdot s)^m f_S(s) ds = Q_s^m \cdot Z \tag{23}$$

where Z is the estimated fatigue load.

Mean loads. The mean load error is of similar nature and origin as that for the stress ranges, but is likely to be different in magnitude. For instance, if stress ranges and mean loads are taken from measurements, signal drift will directly influence the mean loads but not necessarily the dynamic loads (i.e., stress ranges) [23]. We therefore introduce a separate modeling error for the mean loads, and assume that the true mean stress may be expressed as $\sigma'_m = Q_m \cdot \sigma_m$, where Q_m is the mean load error and σ_m is the estimated mean stress. The true representative mean load is then obtained by substituting σ'_m for σ_m in Equation (6):[3]

$$G^*_{1,k}{}' = -\frac{1}{b_1} \log \left[\frac{\sum_i n_i \cdot s_i^m \cdot 10^{-b_1 \cdot g_1(Q_m \cdot \sigma_{m,i})}}{n_{0,k} \cdot \mathrm{E}[S^m]_k} \right] \tag{24}$$

[3]Strictly, the true mean stress S' should also be substituted for the estimated mean stress S in Equation (24). However, the stress range error (Q_s) cancels out since it enters the inner fraction in both numerator and denominator.

where ${G^*_{1,k}}'$ denotes the true representative mean load. This is inconvenient, since the numerator of the inner expression must be re-evaluated for each realization of the random variable Q_m. However, if the mean load function is on the form $g_1(\sigma_m) \propto \sigma_m$, the true representative mean load may be approximated as

$$G^{*\prime}_1 \approx Q_m \cdot G^*_1 \tag{25}$$

where G^*_1 is the estimated representative mean load. A comparison of Equations (24) and (25) is shown in Figure 6 for two realizations q_m of the mean load error with $g_1(\sigma_m) = \lambda_m$, demonstrating that the approximation error introduced by (25) is negligible for the case considered.

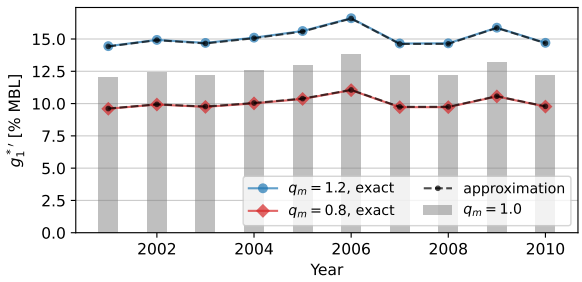

Figure 6: Comparison of true representative mean loads evaluated by Equations (24) ("exact") and (25) ("approximation") for $q_m \in \{0.8, 1.2\}$ with $g_1(\sigma_m) = \lambda_m$ [% MBL], using the joint stress range and mean load distributions applied in Example 1. Representative mean loads for $q_m = 1.0$ are included for reference.

Corrosion grade. A source of corrosion grade error is the categorization from inspections, in particular for the subjective scale used for the model described in Section 2. If a more objective scale were used, with categorization from for instance 3-D scans, the categorization error could be reduced but not fully eliminated.[4] Errors may also arise in the assumptions about the development of the corrosion grade between two inspection events. Analogously to the inclusion of stress range and mean load errors, we assume that the true corrosion grade may be expressed as $C' = Q_c \cdot C$ where Q_c is the corrosion grade categorization error and C is the estimated corrosion grade. The implications for the true representative value of the corrosion grade function, $G^{*\prime}_2$, then depends on the assumed form of the corrosion grade function, $g_2(c)$. For the function described in Section 2 and used in Example 2, $g_c(c) = c$, it is

$${G^*_{2,k}}' = Q_c \cdot C_k \tag{26}$$

where C_k is the estimated corrosion grade for the k^{th} year.

[4]See Gabrielsen et al. [24] for preliminary results from ongoing work, aiming to develop computer algorithms that may be used to determine the corrosion grade based on 3-D scans of the chain links.

Fatigue damage including model uncertainty. An adjusted expression for the weakest link fatigue damage is now obtained by substituting true values $(Z', G_1^{*\prime}, G_2^{*\prime})$ for estimated values (Z, G_1^*, G_2^*) in Equation (21):

$$D_W(\boldsymbol{X}; N_y, N) = \frac{1}{W} \sum_{k=1}^{N_y} \frac{Q_s^m \cdot Z_k}{10^{\left(B_0 + B_1 \cdot Q_m \cdot G_{1,k}^* + B_2 \cdot Q_c \cdot C_k\right)}} \tag{27}$$

where we have assumed that the approximation in (25) holds, and that the representation in (26) is applicable. Note that we have here implicitly assumed that the model uncertainties (Q_s, Q_m, Q_c) take on the same value for all components within a segment.

3.4. Limit state function

A common representation of the failure criterion is in terms of a limit state function, $g(\boldsymbol{X})$, which divides the space of the random variables into a failure domain and a safe domain for the failure mode considered:

$$\begin{aligned} \text{failure domain:} \quad & g(\boldsymbol{x}) \leq 0 \\ \text{safe domain:} \quad & g(\boldsymbol{x}) > 0 \end{aligned} \tag{28}$$

The failure probability may then be expressed as the probability that a realization of the random vector $\boldsymbol{X}$ falls into the failure domain, $p_f = \mathrm{P}\left[g(\boldsymbol{X}) \leq 0\right]$. Hence, based on Equation (22), we define the limit state function for fatigue failure of a chain segment as

$$g(\boldsymbol{X}; N_y, N) = D_{\mathrm{cr}} - D_W(\boldsymbol{X}; N_y, N) \tag{29}$$

where $D_W(.)$ is the fatigue damage of the weakest link as defined in Equation (27). The limit state function for single link failure is then obtained as a special case of (29), with $N = 1$ (in which case $W = R = 10^{\epsilon}$).

3.5. Bounds on the failure of a mooring line

A mooring line is normally composed of more than one segment. The segments may be of the same type (e.g., all studless chains, possibly with different diameters), or they may be composed of different component types (e.g., chains and steel wire rope). In any case, it is a series system for which failure of any one segment leads to line failure. To formulate this, we first define the event E_j to denote fatigue failure for segment j, and $\bar{E}_j$ to denote its complement (the event that segment j survives):

$$\begin{aligned} E_j: \quad & g(\boldsymbol{X}_j; N_y, N_j) \leq 0 \\ \bar{E}_j: \quad & g(\boldsymbol{X}_j; N_y, N_j) > 0 \end{aligned} \tag{30}$$

where N_j is the number of components in segment j. Note that to simplify the notation slightly, we have here assumed that the same limit state function, $g(.)$, is applicable to all segments. In principle, however, it may differ for segments of different component types.

Analogous to Equation (15) describing segment failure, the probability of a mooring line fatigue failure may be expressed either by means of the event that any one segment fails, or by means of the complement of the event that all segments survive:

$$p_{f,\text{line}} = \mathrm{P}\left[\bigcup_{j=1}^{J} E_j\right] = 1 - \mathrm{P}\left[\bigcap_{j=1}^{J} \bar{E}_j\right] \tag{31}$$

where J is the number of segments in the mooring line. In order to proceed from this point we would need to address the partial correlation of the segment failure events. A natural way forward could be to address the dependence or independence between the random variables contained in each random vector $\boldsymbol{X}_j$, similar to what was done for the partial dependence for the segment failure formulation. However, identical assumptions to those made for within segment dependence and independence cannot necessarily be justified. Specifically;

- The S-N model coefficients will differ between segments with different component types.
- The fatigue loads will be highly correlated, but are likely to be of different magnitude due to for instance different component dimensions, damping effects along the line or even different stress range effect (S-N curve slope parameter, m, cf. Equations (1) and (4)).
- Mean loads are also highly correlated, but with magnitudes that depend on segment positions along the line.
- Corrosion grades may be anywhere between highly correlated (e.g., for segments that are close to each other and of similar component types) or completely uncorrelated (e.g., for segments in different positions along the line, such as fairlead chain vs. bottom chain, or for chain segments of different material grades).
- Replacement of individual segments, for any reason, leads to different number of years in service (N_y) between segments.

Hence, mooring line failure cannot be formulated in the same compact form as that for segment failure in the general case.

As an alternative to further developing Equation (31), crude bounds (similar to those discussed in Example 3) may be given as [25, Ch. 5]:

$$\max_{j=1}^{J}\{\mathrm{P}[E_j]\} \leq p_{f,\text{line}} \leq 1 - \prod_{j=1}^{J}\left(1 - \mathrm{P}\left[E_j\right]\right) \tag{32}$$

where the lower bound is exact for fully dependent failure events E_j whereas the upper bound is exact for completely independent events. Note that if the failure events are rare (i.e., $\mathrm{P}[E_j] \ll 1$ for all j), the upper bound may approximated by $p_{f,\text{line}}^{(\text{upper})} \approx \sum_{j=1}^{J} \mathrm{P}[E_j]$. For the general series system these bounds may be too wide to be of any practical value, but not necessarily for a mooring line with a limited number of segments. This is illustrated by the following example.

Example 4. Consider a mooring line composed of $J = 5$ segments, and let $p_{f,j} = \mathrm{P}[E_j]$ denote the marginal probability of failure for segment number j. We first consider a case where one of the segments is more exposed to fatigue than the remaining segments: $p_{f,1} = 10^{-4}$ and $p_{f,j} = 10^{-5}$ for $j \in (2, ..., 5)$. The mooring line failure probability is then bounded by $p_{f,\mathrm{line}} = \left[1.0 \times 10^{-4}, 1.4 \times 10^{-4}\right]$, with a ratio between the upper and lower bounds of 1.4. Next, we consider a case that is perhaps less likely for a mooring line in practice; we assume that all segments are equally exposed to fatigue with marginal failure probabilities $p_{f,j} = 10^{-4}$ for $j \in (1, ..., 5)$. This gives the bounds $p_{f,\mathrm{line}} = \left[1.0 \times 10^{-4}, 5.0 \times 10^{-4}\right]$, with a ratio of 5 between upper and lower bounds.

Firstly, the initial case illustrates that mooring line fatigue failure is likely to be dominated by the critical segment. Secondly; the probability bounds are actually fairly narrow for both the cases in this example, considering that structural reliability calculations are normally concerned with orders of magnitude rather than exact numbers. In any case, the starting point for assessment of mooring line failure probability is to calculate the failure probability for each *segment* properly, and this will be the focus for the remainder of this paper. Note that an extension of a fatigue reliability formulation into considering failure of two mooring lines is presented and discussed by Mathisen and Hørte [4].

3.6. Distribution of weakest link resistance

We will now elaborate on the distribution of W, defined in (17) and describing the deviation from median fatigue capacity for the weakest link in a segment, and used to define the weakest link fatigue damage in Equation (21). Let ϵ be normally distributed with mean μ_ϵ and variance σ_ϵ^2, denoted $\epsilon \sim N(\mu_\epsilon, \sigma_\epsilon^2)$.[5] The random variable $R = 10^\epsilon$ then follows a lognormal distribution, denoted $R \sim LN(\mu_{\ln R}, \sigma_{\ln R})$, which is defined by

$$f_R(r\,;\,\mu_{\ln R}, \sigma_{\ln R}) = \frac{1}{r \cdot \sigma_{\ln R} \cdot \sqrt{2\pi}} \exp\left[-\frac{1}{2}\left(\frac{\ln r - \mu_{\ln R}}{\sigma_{\ln R}}\right)^2\right] \tag{33}$$

$$F_R(r\,;\,\mu_{\ln R}, \sigma_{\ln R}) = \Phi\left(\frac{\ln r - \mu_{\ln R}}{\sigma_{\ln R}}\right) \tag{34}$$

where $f_R(.)$ is the probability density function (PDF) and $F_R(.)$ is the cumulative distribution function (CDF). The parameters $\mu_{\ln R}$ and $\sigma_{\ln R}$ correspond to respectively mean value and standard deviation of the normal variate $\ln R$, and $\Phi(.)$ is the standard normal CDF. The distribution parameters for R may then be obtained from

$$\mu_{\ln R} = \mathrm{E}[\ln R] = \ln 10\ \mu_\epsilon \tag{35}$$

$$\sigma_{\ln R} = \sqrt{\mathrm{Var}[\ln R]} = \ln 10\ \sigma_\epsilon \tag{36}$$

[5] Strictly, following the regression model in Equation (3), we have $\mu_\epsilon := 0$. However, for the generality of the current subsection, we prefer to maintain the possibility for a non-zero μ_ϵ.

As previously noted, the *exact* distribution of $W = \min\{R_1, \ldots, R_N\}$ is obtained from order statistics, see e.g., [19], as:

$$f_W(w; N) = N\,[1 - F_R(w)]^{N-1}\, f_R(w) \tag{37}$$

$$F_W(w; N) = 1 - [1 - F_R(w)]^N \tag{38}$$

where $f_R(.)$ and $F_R(.)$ are respectively the PDF and the CDF of the underlying distribution (for a single link). Note that (37) and (38) are exact regardless of the underlying distribution type.

When the underlying distribution is lognormal, the distribution of the weakest link asymptotically (as $N \to \infty$) approaches the type III extreme value distribution of minima (Weibull) [19]. The Weibull distribution is defined by

$$f_W(w;\, \alpha, \gamma) = \frac{\gamma}{\alpha}\left(\frac{w}{\alpha}\right)^{\gamma-1} \exp\left[-\left(\frac{w}{\alpha}\right)^{\gamma}\right] \tag{39}$$

$$F_W(w;\, \alpha, \gamma) = 1 - \exp\left[-\left(\frac{w}{\alpha}\right)^{\gamma}\right] \tag{40}$$

where α and γ are scale and shape parameters, respectively. These distribution parameters may be obtained from those of the underlying distribution as [26]

$$\alpha = e^{\,\mu_{\ln R} - a_n\, \sigma_{\ln R}} = 10^{\,\mu_\epsilon - a_n\, \sigma_\epsilon} \tag{41}$$

$$\gamma = \frac{1}{b_n\, \sigma_{\ln R}} = \frac{1}{b_n\, \ln 10\, \sigma_\epsilon} \tag{42}$$

where the coefficients a_n and b_n are functions of the number of links, and given by [26]

$$a_n = \frac{2\ln N - 0.5\ln(\ln N) - \ln(2\sqrt{\pi})}{\sqrt{2\ln N}} \tag{43}$$

$$b_n = \frac{1}{\sqrt{2\ln N}} \tag{44}$$

In many cases, using the exact distribution in (38) for numerical calculations is straightforward. However, the Weibull distribution in (40) may be easier to work with and is commonly available in software for probabilistic analysis. The following example illustrates the effect of the number of links on the weakest link resistance, and also that the asymptotic distribution may be a reasonable approximation even for a finite number of components.

Example 5. Consider a case with $\epsilon \sim N(0, 0.17^2)$, which corresponds to the S-N models in Table 1. The single link distribution is then $R \sim LN(0, 0.39)$. The exact and asymptotic distributions of W are shown in Figure 7 for three different segment sizes, along with the lognormal distribution for a single link. Distribution statistics are listed in Table 2. These clearly show that when the segment size (N) increases, the distribution is shifted towards lower resistance and becomes more narrow. Reasonable agreement is observed between the exact and the asymptotic (Weibull) distributions, including the lower regions (left

tails) of the distributions. For instance, the difference in 1-percentile is around 10% for $N = 20$ and roughly 5% for $N = 500$ with the asymptotic distribution on the low side.

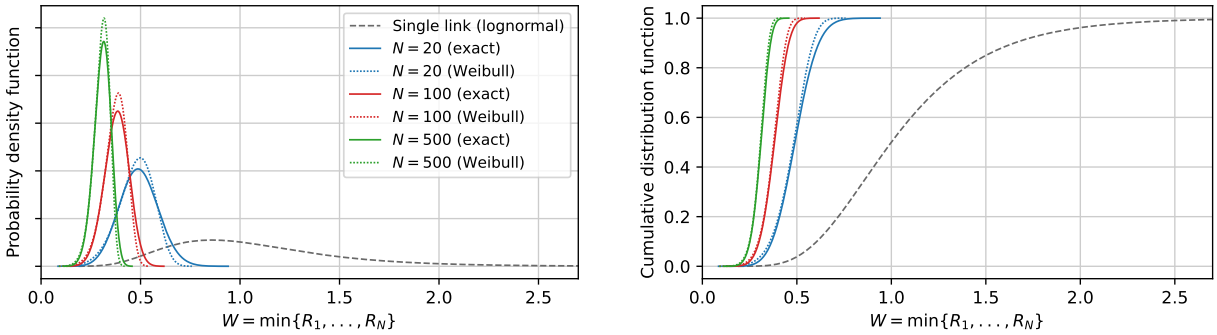

(a) Probability density function (PDF).

(b) Cumulative distribution function (CDF).

Figure 7: Example of weakest link resistance for $N \in \{20, 100, 500\}$: exact distribution vs. asymptotic Weibull distribution, for $\epsilon \sim N(0, 0.17^2)$. Single link distribution included for comparison.

Table 2: Statistics for W from Example 5.

	Exact					Asymptotic
N	Median	Mean	St.dev.	CoV	p1	p1
1[a]	1.00	1.08	0.44	0.41	0.40	–
20	0.49	0.49	0.10	0.20	0.28	0.25
100	0.38	0.38	0.06	0.16	0.23	0.22
500	0.31	0.31	0.04	0.14	0.20	0.19

St.dev.: standard deviation. CoV: coefficient of variation. p1: 1-percentile.

[a] Single link, i.e., $W = R$.

3.7. On the correlation between Z and G_1^*

The fatigue load (Z) and the representative mean load (G_1^*) originate from the same underlying load process, and may therefore be correlated with each other. Results presented in [13, Sec. 3] for a typical production system in the Norwegian Sea showed that for each mooring line, the sign and magnitude of this correlation depend on its orientation compared to the dominating directions of environmental loads. Consequently, if the annual variability of Z and G_1^* is of importance for the problem at hand, the correlation between them may be important as well. In the following we will present three alternative ways to address this in the reliability calculations.

The first option it to model Z and G_1^* as dependent random variables. The practical implications of this approach will depend on the choice of method for dependence modeling and the calculation method for the

reliability problem.

A second alternative is to introduce the random variable $Z^* = Z \cdot 10^{-B_1 \cdot G_1^*}$ as an "effective" fatigue load that includes the mean load effect on the capacity, as proposed in [13]. A probabilistic model for the variability of Z^* may then be established from joint statistics of Z and G_1^*, implicitly accounting for the correlation between them. However, two premises are necessary for this approach to be useful. Firstly, the mean load coefficient (B_1) should be modeled as fixed. Otherwise, the probabilistic model for Z^* will depend on the random variable B_1, in which case the introduction of Z^* offers no convenience over modeling the correlation between Z and G_1^* as described in the first alternative. Secondly, inclusion of model uncertainties for stress ranges and mean loads to obtain the true value of the effective fatigue load yields $Z^{*\prime} = Q_s^m \cdot Z \cdot 10^{-B_1 \cdot Q_m \cdot G_1^*}$ (assuming that the approximation in Equation (25) is applicable). That is, the true effective fatigue load ($Z^{*\prime}$) cannot be expressed as an explicit function of the estimated effective fatigue load (Z^*) unless a fixed value is assumed for the mean load error (Q_m). A possible remedy could be to set a fixed value for the mean load error (typically, $Q_m = 1$), and substitute an alternative model uncertainty Q_{se} for Q_s to represent the total model error for the effective fatigue load. This new model uncertainty, Q_{se}, cannot be determined directly from Q_s and Q_m, and would then need to be estimated separately.

Finally, a third alternative is to neglect the dependence between Z and G_1^* and model them as mutually independent variable. This may be justified if (i) the correlation between them is weak, or (ii) the annual variability of Z and G_1^* is shown to be of limited importance for the quantity of interest, or (iii) the correlation between Z and G_1^* is found to be negative (if the correlation between them is negative, implying that a high fatigue load is likely to be combined with a low mean load, the assumption of independence will be conservative with respect to fatigue damage). Note that this third approach, assuming independence, will be applied in the case study in Section 4.

3.8. Summary

Starting from the failure criterion for single link failure in Equation (8), we have developed a fatigue reliability model for mooring chain segment failure that includes the effect of mean load and degradation due to corrosion. A fundamental assumption for the current formulation of segment failure is that the random variables may be divided into two groups as follows: (i) variables that are fully correlated and each takes on the same value for links within a segment (dynamic loads, mean loads, corrosion grade, S-N model coefficients and model uncertainties), and (ii) variables that are independent across links within a segment (S-N model regression error). The resulting limit state function for segment failure is given in Equation (29), which is expressed in terms of the fatigue damage of the weakest link and includes single link failure as a special case. The weakest link is identified as the one with the largest negative realization of the S-N model error, that is, the link with the least favorable deviation from the median fatigue capacity.

4. Case study

The reliability formulation developed in Section 3 is now applied for a case study. First, the scope and the basis for the study are described. Then, the calculation methods applied are outlined. Finally, results are presented and discussed, and some main conclusions of the case study are summarized.

4.1. Scope and objectives

We consider fatigue of a mooring chain segment, and the case study is divided into three parts:

1. A *global sensitivity analysis*, to (a) identify random variables that may be fixed in order to simplify the model and reduce the dimension of the problem, and (b) assess the importance of interactions between random variables in the model.
2. A *reliability analysis*, to (a) calculate the probability of fatigue failure for the base case, (b) validate the selected approach, and (c) assess the importance of the respective variables compared to the results from the global sensitivity analysis.
3. A *parametric study*, to demonstrate the impact on failure probability from (a) alternative cases such as higher fatigue loads or mean loads and (b) alternative S-N models neglecting mean load or corrosion effects.

4.2. Basis

The base case is defined as follows:

- A service life of 15 years.
- The segment consists of 500 chain links.
- Fatigue capacity described by a S-N model with stress range effect $m = 3$, and intercept parameter according to Equation (2) with $g_1(\sigma_m) = \lambda_m$ [% MBL] and $g_2(c) = c$.

Probability distributions applied for the random variables in the base case are listed in Table 3, and are defined on the basis described in the subsequent paragraphs. The base case is partly related to the case study presented in [13], but with higher fatigue loads. The idea is that it will be more interesting to assess interaction effects and the influence of main parameters for a case with failure probability closer to a minimum acceptable safety level.

Critical damage. Wirsching and Chen [27] list statistics for the uncertainty in Miner's sum at failure from various sources, with median values ranging from 0.69 to 1.15 and coefficient of variation (CoV) ranging from 0.19 to 0.67. In their example of tendon fatigue for a tension-leg platform they modeled it as a lognormal variable with a median value of 1.0 and a CoV of 0.30. This model has since been widely used for fatigue

Table 3: Random variables for base case.

Variable	Symbol	Unit	Dimension[a]	Distributed as	Mean	St.dev.	CoV[b]
Miner's sum at failure	D_{cr}	-	1	$LN(0, 0.29)$	1.04	0.31	0.30
Predictive uncertainty of S-N model	ϵ	-	1	$N(0, 0.17^2)$	0	0.17	-
Time-invariant term of S-N intercept	B_0	-	1	see note[c]	12.249	0.088	-
Mean load effect	B_1	-	1	see note[c]	-0.0507	0.0045	-
Corrosion grade effect	B_2	-	1	see note[c]	-0.106	0.0075	-
Annual fatigue loads	Z	MPa^3	N_y	$LN(19.96, 0.39)$	5×10^8	2×10^8	0.40
Annual representative mean loads	G_1^*	% MBL	N_y	$N(15.0, 0.6^2)$	15.0	0.6	0.04
Corrosion grade at end of service life	C_{end}	-	1	$U(1, 7)$	4	1.7	-
Model uncertainty (stress ranges)	Q_s	-	1	$N(1.0, 0.10^2)$	1.0	0.10	0.10
Model uncertainty (mean loads)	Q_m	-	1	$N(1.0, 0.10^2)$	1.0	0.10	0.10
Model uncertainty (corrosion grade)	Q_c	-	–	Fixed	1.0	-	-

Dimension: number of random variables. St.dev.: standard deviation. CoV: coefficient of variation.

[a] Number of i.i.d. random variables with this distribution.

[b] CoV is given when used to define the distribution.

[c] Multivariate normal with covariance matrix given in Equation (45). Listed standard deviations correspond to the square roots of the diagonal terms of the covariance matrix.

reliability of marine structures, including the DNVGL-OS-E301 design code calibration [4] and the JCSS probabilistic code for fatigue [28], and is also used for D_{cr} in the present study.[6]

Weakest link resistance. The weakest link resistance, W, is here defined indirectly by means of the S-N model regression error, ϵ, representing deviation from the median fatigue capacity of individual links. The model is identical to that applied for Example 5 in Section 3.6. For the calculations in the present study, the exact distribution of W as defined in Equation (38) is used.

S-N model intercept coefficients. The uncertainty in the coefficients of the S-N model intercept parameter, $(B_j)_{j\in\{0,1,2\}}$, represents the inferential uncertainty [see e.g., 14] of the regression model in Equation (3). They are jointly distributed according to a multivariate normal distribution, $N(\boldsymbol{\mu}, \boldsymbol{\Sigma})$, with mean vector $\boldsymbol{\mu}$ defined from the least-squares estimates in Table 1 and covariance matrix [13]

$$\boldsymbol{\Sigma} = \begin{bmatrix} 7.770\times10^{-3} & -3.829\times10^{-4} & -4.453\times10^{-4} \\ -3.829\times10^{-4} & 2.046\times10^{-5} & 1.714\times10^{-5} \\ -4.453\times10^{-4} & 1.714\times10^{-5} & 5.612\times10^{-5} \end{bmatrix} \tag{45}$$

[6] Strictly, JCSS [28] suggests that the Miner's sum uncertainty is modeled as lognormal with *mean* 1.0, whereas Wirsching and Chen [27] suggested a *median* value of 1.0. The latter is adopted here, and corresponds to a mean value of 1.04 with a CoV of 0.30.

In [13], the inferential uncertainty of the B_j coefficients was found to be non-influential for the fatigue damage of the lines considered. This will be reassessed in the present study, including the importance of possible interactions with other random variables.

Fatigue loads. The probability distribution assigned to Z represents the annual variability of the fatigue loads, hence, N_y i.i.d. random variables are needed to model the fatigue damage after N_y years. The expected value is increased compared to those reported for the mooring system considered in [13], and is here set to $E[Z] = 5 \times 10^8$. This is the maximum annual fatigue load that meets the design code requirements in DNVGL-OS-E301 [2] with a fatigue safety factor of 8 without accounting for corrosion in any way.[7] The underlying calculations to obtain this value are given in Appendix A. For the mooring lines considered in [13], the CoV of Z was found to be in the range 0.24–0.38. For the base case of the present study we set the CoV to 0.40, just above the upper value of the given range. The annual fatigue loads are assumed to follow a lognormal distribution, based on the test-of-fit results reported in [13].

Representative mean loads. As for the fatigue loads, the probability distribution assigned to G_1^* represents the annual variability of the representative mean load. For the present study we assume an expected value of 15 [% MBL] and a CoV of 0.04. The mean value is slightly higher than that reported for the mooring lines considered in [13]. However, the mean load is sensitive to parameters such as chain dimension and material grade, operational measures (e.g., pretension), type of unit and orientation of line, so any value from 10% to 20% (or even outside this range in certain cases) is of relevance for the study. The selected CoV is in the high end of the range reported in [13] (0.02–0.04). For convenience, the annual mean loads are assumed to follow a normal distribution. Furthermore, they are assumed to be independent of the annual fatigue loads, which implies that the possible correlation between them is neglected. This latter choice will be assessed in connection with the global sensitivity analysis.

Corrosion grade. We assume that nothing is known about the corrosion grade of the segment, either because the assessment is performed prior to operation or because inspections have not been carried out. The only information available is then that the grade is bounded by its value at installation ($c = 1$) and what is presently considered as the upper limit of the corrosion grade scale ($c = 7$). One could imagine that more narrow bounds for the most likely corrosion grade development could be defined based on previous experience for similar chain segments (e.g., comparable depth and location along line), but this is not addressed here. Hence, the corrosion grade at the end of the service life, C_{end}, is modeled as a uniform variable with support $[1, 7]$, in accordance with the maximum entropy principle [29]. The temporal development is assumed to be described by Equation (7) in Example 2, with parameters $a = 0.5$, $\eta = 1.0$ and $L = 15$.

[7] The relation between the expected annual fatigue load and the design code requirements is given for convenience, and should not be interpreted as an attempt to quantify the safety level inherent in DNVGL-OS-E301 [2].

Model uncertainties. The model uncertainties may be hard to quantify, as they represent deviation between the estimated and the true (and generally unknown) values. We here apply normal distributions with a mean of 1.0 and a CoV of 0.10 to model the uncertainty in both stress ranges and mean loads (Q_s and Q_m, respectively). This is comparable in magnitude to the model uncertainties applied in [4] (although they are included in the reliability model in different ways). In general, if the basis for quantifying the model uncertainties is poorly justified and the reliability calculations demonstrate a sensitivity to these variables, an effort to improve the basis for quantification is recommendable. For corrosion grade, the model uncertainty is here fixed to 1.0. The rationale is that in the present study, we have already modeled complete ignorance about the value of the corrosion grade, C_{end}.

Model dimension and dependence between variables. In summary, the base case probabilistic model has a dimension of $8 + 2 \cdot N_y$, that is, 38 random variables are used to evaluate the limit state function at the end of the service life of 15 years. These random variables are all assumed to be mutually independent, except for the B_j coefficients of the S-N model which are jointly distributed according to a multivariate normal distribution.

4.3. Method

The methods applied for the case study are now described. We first outline the sensitivity measures and corresponding estimators used for the global sensitivity analysis, then describe each step of the reliability analysis performed for the present work. The objective of the reliability analysis is to calculate the probability of failure, p_f, by computing

$$p_f = \mathrm{P}[g(\boldsymbol{X}) \leq 0] = \int_{g(\boldsymbol{X}) \leq 0} f_{\boldsymbol{X}}(\boldsymbol{x})\, d\boldsymbol{x} \tag{46}$$

where $g(\boldsymbol{X})$ is the limit state function given in Equation (29) and $f_{\boldsymbol{X}}(.)$ is the joint PDF for the random vector $\boldsymbol{X}$. For the present study, we first approximate (46) through performing a FORM (first-order reliability method) analysis. The FORM result is then used as the basis for estimating the integral more accurately by means of importance sampling. A byproduct of FORM is a set of sensitivity measures referred to as importance factors, which are described thereafter. We close this subsection by briefly addressing the difference between the accumulated and the annual probability of fatigue failure.

4.3.1. Global sensitivity analysis

Consider the output of a generic model, $Y = f(\boldsymbol{X})$, where $\boldsymbol{X} = (X_1, X_2, \ldots, X_M)$ is a random vector of size M. In the context of the present study, the model $f(.)$ may be the fatigue damage in Equation (21) or the limit state function in Equation (29), and $\boldsymbol{X}$ contains the random variables in Table 3. A global sensitivity analysis is concerned with quantifying the impact on the uncertainty of Y from the uncertainty of each of the components, X_i, over the entire range of possible outcomes.

We here employ a set of variance-based sensitivity indices, commonly known as *Sobol' indices* after his work on variance-based sensitivity measures [e.g., 30]. The brief outline given below is based on Saltelli et al. [31].

Assuming that the components in $\boldsymbol{X}$ are mutually independent, a variance-based first-order sensitivity index is

$$S_i = \frac{\mathrm{Var}_{X_i}(\mathrm{E}_{\boldsymbol{X}_{\sim i}}[Y|X_i])}{\mathrm{Var}(Y)} \tag{47}$$

where Var(.) denotes variance and E[.] is the expectation. The subscript $\cdot_{X_i}$ means that the variance (or expectation) is taken over the range of possible outcomes for component X_i, whereas subscript $\cdot_{\boldsymbol{X}_{\sim i}}$ means that it is taken over the range of possible outcomes for all components except X_i. Hence, the first-order index in (47) is a measure of the variance of the conditional expectation of Y given X_i, over the range of X_i, normalized with respect to the total variance $\mathrm{Var}(Y)$. In other words; it quantifies the proportion of the uncertainty in Y that may be attributed to the uncertainty in X_i alone, and is a number between 0 and 1.

A related sensitivity measure is the total effect index:

$$S_{Ti} = 1 - \frac{\mathrm{Var}_{\boldsymbol{X}_{\sim i}}(\mathrm{E}_{X_i}[Y|\boldsymbol{X}_{\sim i}])}{\mathrm{Var}(Y)} = \frac{\mathrm{E}_{\boldsymbol{X}_{\sim i}}(\mathrm{Var}_{X_i}[Y|\boldsymbol{X}_{\sim i}])}{\mathrm{Var}(Y)} \tag{48}$$

which quantifies the total contribution from uncertainty in X_i to the variance of Y, including interactions with other random variables. For a purely additive model, we have $S_{Ti} = S_i$ and $\sum_i S_i = 1$. The quantity $1 - \sum_i S_i$ may therefore be used to quantify the proportion of the variance that is caused by non-additive interactions in the model. Furthermore, zero total effect ($S_{Ti} = 0$) is a necessary and sufficient condition for X_i to be non-influential. Hence; given $S_{Ti} = 0$, the random variable X_i may be fixed to any value without affecting the variance of Y.

Note that the index i may be replaced by a vector referring to a group of components, $\boldsymbol{X_i}$. The sensitivity indices $(S_{\boldsymbol{i}}, S_{T\boldsymbol{i}})$ then quantify the effect of this group of components combined. Also, in case the requirement of independent variables is not fully satisfied, independence may be achieved by grouping interdependent components [32]. For instance, for the random variables in Table 3, the S-N model coefficients (B_0, B_1, B_2) may be grouped to obtain independence from the remaining variables.

In practice, S_i and S_{Ti} may be estimated by Monte Carlo simulation (MCS). The sampling scheme and estimators adapted for the present study are from Saltelli et al. [33]:

$$\mathrm{Var}_{X_i}(\mathrm{E}_{\boldsymbol{X}_{\sim i}}[Y|X_i]) = \frac{1}{N_{\mathrm{MC}}} \sum_{j=1}^{N_{\mathrm{MC}}} f(\boldsymbol{B})_j \left(f(\boldsymbol{A}_{\boldsymbol{B}}^{(i)})_j - f(\boldsymbol{A})_j \right) \tag{49}$$

$$\mathrm{E}_{\boldsymbol{X}_{\sim i}}(\mathrm{Var}_{X_i}[Y|\boldsymbol{X}_{\sim i}]) = \frac{1}{2N_{\mathrm{MC}}} \sum_{j=1}^{N_{\mathrm{MC}}} \left(f(\boldsymbol{A})_j - f(\boldsymbol{A}_{\boldsymbol{B}}^{(i)})_j \right)^2 \tag{50}$$

$$\mathrm{Var}(Y) = \frac{1}{N_{\mathrm{MC}}} \sum_{j=1}^{N_{\mathrm{MC}}} f(\boldsymbol{A})_j^2 - \left(\frac{1}{N_{\mathrm{MC}}} \sum_{j=1}^{N_{\mathrm{MC}}} f(\boldsymbol{A})_j \right)^2 \tag{51}$$

where $\boldsymbol{A}$ and $\boldsymbol{B}$ are $N_{\mathrm{MC}} \times M$ sample matrices (i.e., for each of them, column i contains a sample with N_{MC} realizations of component X_i); $\boldsymbol{A}_{\boldsymbol{B}}^{(i)}$ is matrix $\boldsymbol{A}$ with column i replaced by the corresponding column from $\boldsymbol{B}$; and $f(.)_j$ should be interpreted as a model evaluation for the sample in row j of the argument (e.g., $f(\boldsymbol{A})_j$ refers to a model evaluation for row j of $\boldsymbol{A}$). In total, $N_{\mathrm{MC}} \times (M+2)$ model evaluations are needed to estimate S_i and S_{Ti} for all M components by these estimators. Alternative methods using surrogate models of $f(.)$ exist, such as the one presented by Sudret [34].

4.3.2. FORM analysis

The FORM procedure is now outlined. For further details, see e.g., [20, 25].

The first step of the FORM analysis is the isoprobabilistic transformation

$$\boldsymbol{U} = T(\boldsymbol{X}) \tag{52}$$

where $T(.)$ denotes a transformation from the random vector $\boldsymbol{X} \in \mathbb{R}^M$ in physical space to an independent standard normal vector $\boldsymbol{U} \in \mathbb{R}^M$; that is, $U_i \sim N(0,1)$ for $i \in \{1, ..., M\}$. If the random variables in $\boldsymbol{X}$ are mutually independent, the transformation may be performed independently for each component X_i:[8]

$$U_i = T_i(X_i) \tag{53}$$

For a given value u_i or x_i, this transformation (or its inverse) is then constructed by requiring $\Phi(u_i) = F_{X_i}(x_i)$, such that

$$u_i = \Phi^{-1}(F_{X_i}(x_i)) \;\longleftrightarrow\; x_i = F_{X_i}^{-1}(\Phi(u_i)) \tag{54}$$

where $\Phi(.)$ is the standard normal CDF and $F_{X_i}(.)$ is the CDF of component X_i. The limit state function may now be computed for a point in the transformed U-space by evaluating

$$g_{\boldsymbol{U}}(\boldsymbol{u}) = g(T^{-1}(\boldsymbol{u})) \tag{55}$$

The second step in the FORM analysis is identification of the *design point*, which is the point in the failure domain with the shortest distance to the origin of the standard normal space:

$$\boldsymbol{u}^* = \arg\min \{ \|\boldsymbol{u}\| \,;\; g_{\boldsymbol{U}}(\boldsymbol{u}) \leq 0 \} \tag{56}$$

See Figure 13 in Section 4.4 for an illustration of the design point. Equation (56) is a constrained minimization problem that may be solved by for instance the HLRF (Hasofer-Lind-Rackwitz-Fiessler) algorithm [35], the improved version by Zhang and Der Kiureghian [36] (often referred to as the iHLRF algorithm), or by general optimization routines that are fit for purpose (e.g., `scipy.optimize.minimize(method='SLSQP')` [37]). For the present work, the iHLRF algorithm is implemented.

[8] For dependent variables, the transformation to standard normal space must be performed by alternative techniques such as for instance the Rosenblatt or Nataf transformations, see e.g., [20, 25].

The FORM reliability index, also known as the Hasofer-Lind index, is defined as the distance from the origin of the U-space to the design point:

$$\beta = \|\boldsymbol{u}^*\| \tag{57}$$

and is related to the probability of failure through

$$p_{f,\mathrm{FORM}} = \Phi(-\beta) \tag{58}$$

in which the limit state surface is implicitly approximated by a tangent hyperplane at $\boldsymbol{u}^*$. Hence, FORM is exact only if the limit state surface is linear in U-space, and the accuracy of the approximation depends on its shape at the design point and the dimension of the problem [20, pp. 173 and 214].

4.3.3. Importance sampling

The integral in (46) may be rewritten to formulate the probability of failure as

$$p_f = \int_{\boldsymbol{X}} \mathbb{I}_{g(\boldsymbol{x})\leq 0}(\boldsymbol{x})\, f_{\boldsymbol{X}}(\boldsymbol{x})\, d\boldsymbol{x} \tag{59}$$

where $\mathbb{I}$ is the indicator function. An unbiased estimate of this integral may be obtained from MCS, and the crude MCS estimate is

$$\hat{p}_{f,\mathrm{MC}} = \frac{1}{N_{\mathrm{MC}}} \sum_{j=1}^{N_{\mathrm{MC}}} \mathbb{I}_{g(\boldsymbol{x})\leq 0}(\boldsymbol{x}_j) \tag{60}$$

where N_{MC} is the sample size and $\boldsymbol{x}_j$ is the j^{th} random sample of $\boldsymbol{X}$. The convergence of the crude MCS is slow, in particular for low failure probabilities, resulting in high variance estimates. An effective variance reduction technique is the simulation procedure known as importance sampling (IS). Instead of sampling from the joint distribution of the random variables, $f_{\boldsymbol{X}}(.)$, samples are drawn from a separate sampling distribution, denoted $h_{\boldsymbol{X}}(.)$. By noting that (59) may be written as

$$p_f = \int_{\boldsymbol{X}} \mathbb{I}_{g(\boldsymbol{x})\leq 0}(\boldsymbol{x})\, \frac{f_{\boldsymbol{X}}(\boldsymbol{x})}{h_{\boldsymbol{X}}(\boldsymbol{x})}\, h_{\boldsymbol{X}}(\boldsymbol{x})\, d\boldsymbol{x} \tag{61}$$

the IS estimate of the failure probability is obtained from

$$\hat{p}_{f,\mathrm{IS}} = \frac{1}{N_{\mathrm{MC}}} \sum_{j=1}^{N_{\mathrm{MC}}} \left\{ \mathbb{I}_{g_{\boldsymbol{X}}(\boldsymbol{x})\leq 0}(\boldsymbol{x}_j)\, \frac{f_{\boldsymbol{X}}(\boldsymbol{x}_j)}{h_{\boldsymbol{X}}(\boldsymbol{x}_j)} \right\} \tag{62}$$

where the fraction $f_{\boldsymbol{X}}(\boldsymbol{x}_j)/h_{\boldsymbol{X}}(\boldsymbol{x}_j)$ may be interpreted as a weighting function accounting for the use of a sampling distribution that deviates from $f_{\boldsymbol{X}}(.)$. The efficiency of IS may significantly surpass that of crude MCS if the sampling distribution is wisely selected: a good choice for $h_{\boldsymbol{X}}(.)$ is considered to be a multivariate and independent normal distribution, centered at the FORM design point and with standard deviations equal to those of each variable X_i [25]. For the present work, the sampling is performed in

U-space with sampling distribution $h_{\boldsymbol{U}}(.) = N(\boldsymbol{u}^*, \boldsymbol{I}_M)$, where $\boldsymbol{I}_M$ is an $M \times M$ identity matrix. The failure probability is thus estimated from

$$\hat{p}_{f,\mathrm{IS}} = \frac{1}{N_{\mathrm{MC}}} \sum_{j=1}^{N_{\mathrm{MC}}} \left\{ \mathbb{I}_{g_{\boldsymbol{U}}(\boldsymbol{u}) \leq 0}(\boldsymbol{u}_j) \, \frac{\phi_M(\boldsymbol{u}_j)}{\phi_M(\boldsymbol{u}_j - \boldsymbol{u}^*)} \right\} \tag{63}$$

where $\phi_M(.)$ denotes a multivariate and independent standard normal PDF. A corresponding estimate for the sampling variability of $\hat{p}_{f,\mathrm{IS}}$ is [20]

$$\mathrm{Var}[\hat{p}_{f,\mathrm{IS}}] \approx \frac{1}{N_{\mathrm{MC}} - 1} \left(\frac{1}{N_{\mathrm{MC}}} \sum_{j=1}^{N_{\mathrm{MC}}} \left\{ \mathbb{I}_{g_{\boldsymbol{U}}(\boldsymbol{u}) \leq 0}(\boldsymbol{u}_j) \, \left(\frac{\phi_M(\boldsymbol{u}_j)}{\phi_M(\boldsymbol{u}_j - \boldsymbol{u}^*)} \right)^2 \right\} - \hat{p}^2_{f,\mathrm{IS}} \right) \tag{64}$$

which may be used to verify that the CoV of the estimated failure probability is acceptable.

4.3.4. FORM-based sensitivity measures

The design point may also be expressed as

$$\boldsymbol{u}^* = \beta \boldsymbol{\alpha} \tag{65}$$

where $\boldsymbol{\alpha} = (u_1^*/\beta, \ldots, u_M^*/\beta)$ is a vector containing directional cosines.[9] It also represents the normal vector of the limit state surface at the design point under the FORM assumption, and it follows from (57) that $\|\boldsymbol{\alpha}\| = \boldsymbol{\alpha}^T \boldsymbol{\alpha} = 1$, and $\beta = \boldsymbol{\alpha}^T \boldsymbol{u}^*$. Hence:

$$\left. \frac{\partial \beta}{\partial u_i} \right|_{\boldsymbol{u} = \boldsymbol{u}^*} = \alpha_i \tag{66}$$

which means that α_i is a local measure of the sensitivity of the reliability index to the uncertainty in u_i, evaluated at the design point. This sensitivity measure is referred to as the FORM *importance factors*, and is commonly presented in terms of its squared value, α_i^2. The interpretation of α_i^2 is as follows. The linear approximation to the limit state function in U-space may be expressed as

$$g_{\boldsymbol{U},l}(\boldsymbol{u}) = \nabla g_{\boldsymbol{U}}(\boldsymbol{u}^*)^T (\boldsymbol{u} - \boldsymbol{u}^*) = \|\nabla g_{\boldsymbol{U}}(\boldsymbol{u}^*)\| \, (\beta - \boldsymbol{\alpha}^T \boldsymbol{u}) \tag{67}$$

where $\nabla g_{\boldsymbol{U}}(\boldsymbol{u}^*)$ is the gradient vector of the limit state function evaluated at $\boldsymbol{u}^*$, and we have utilized that $\boldsymbol{\alpha}$ is a unit vector which is parallel to the gradient at this point, $\boldsymbol{\alpha} = -\nabla g_{\boldsymbol{U}}(\boldsymbol{u}^*)/\|\nabla g_{\boldsymbol{U}}(\boldsymbol{u}^*)\|$. The variance of $g_{\boldsymbol{U},l}(\boldsymbol{u})$ is $\mathrm{Var}[g_{\boldsymbol{U},l}(\boldsymbol{u})] = \|\nabla g_{\boldsymbol{U}}(\boldsymbol{u}^*)\|^2 \, \boldsymbol{\alpha}^T \boldsymbol{\alpha} = \|\nabla g_{\boldsymbol{U}}(\boldsymbol{u}^*)\|^2 \sum_i \alpha_i^2$. Hence; α_i^2 describes the proportion of the variance of the linearized limit state function that is caused by the uncertainty in U_i [38]. When the random variables are independent in physical space, there is a one-to-one relation between U_i and X_i, and this interpretation of α_i^2 is valid also for the importance of X_i. Recently, Papaioannou and Straub [39] noted

[9] With the definition in (65), the vector $\boldsymbol{\alpha}$ points into the failure domain. Some authors define $\boldsymbol{\alpha}$ in the opposite direction, in which case $\boldsymbol{u}^* = -\beta\boldsymbol{\alpha}$. See e.g., [20, 25].

that α_i^2 corresponds to the first-order Sobol' index for the effect of U_i on the linearized limit state function and – since $g_{\boldsymbol{U},l}(\boldsymbol{u})$ is purely additive – it is also equal the total effect index.

The *omission sensitivity factors* introduced by Madsen [38] represent another set of FORM-based sensitivity measures. They quantify the relative change in the reliability index if the random variable X_i is replaced by a fixed value. Specifically; for independent variables in physical space, the change in reliability index if X_i is replaced by its mean value is [38]:

$$\frac{\beta(X_i = \mu_{X_i})}{\beta} = \frac{1}{\sqrt{1-\alpha_i^2}} \tag{68}$$

No large error is therefore made in estimation of the reliability index by fixing variables associated with small values of α_i^2.

4.3.5. Accumulated vs. annual failure probability

The failure probability considered for the present work is on the form $p_f = \mathrm{P}[g(\boldsymbol{X};t) \leq 0]$, where t denotes time. In general, this quantity describes the point-in-time failure probability, and neglects the possibility that failure may have occurred at any point in time prior to t (i.e., that the event $g(\boldsymbol{X};t') \leq 0$ may have occurred for $t' < t$) [40]. However; the limit state function for fatigue (based on the S-N approach) will decrease monotonically. The point-in-time probability expressed through the limit state function defined in (29), $p_f = \mathrm{P}[g(\boldsymbol{X};N_y,N) \leq 0]$, therefore represents an *accumulated* probability of failure for all years up to and including year N_y.

Design codes such as DNVGL-OS-E301 [2] are usually calibrated towards a target *annual* probability of failure. Following [4], the annual failure probability may be expressed as the increase in accumulated probability from the year before, conditional on survival prior to the year considered. By introducing the notation $p_f(N_y) = \mathrm{P}[g(\boldsymbol{X};N_y,N) \leq 0]$ for the accumulated probability, this annual probability of failure is

$$p_{f,\mathrm{annual}} = \frac{p_f(N_y) - p_f(N_y-1)}{1 - p_f(N_y-1)} \tag{69}$$

Equation (69) may be viewed as a discrete approximation to the hazard function [e.g., 40], with year as the time unit, describing the annual failure rate conditional on survival up to and including $N_y - 1$ years.

4.4. Results and discussion

4.4.1. Global sensitivity analysis

We start by the global sensitivity analysis, to identify variables that may be fixed, and to assess the importance of interaction effects. Sobol' indices have been estimated for the base case using MCS with $N_{\mathrm{MC}} = 10^6$, and are presented in Figure 8. The variance of the limit state function (Figure 8a) is largely dominated by the uncertainty in critical fatigue damage (D_{cr}), making it hard to assess the importance of the remaining variables. An additional MCS is therefore performed to obtain Sobol' indices for the fatigue

damage of the weakest link (Figure 8b). For the latter simulations, the following random variables have been grouped so that the indices represent the effect of more than one variable: B_j represents (B_0, B_1, B_2) which are grouped to achieve independence, G_1 represents $(G^*_{1,k})_{k\in\{1,\ldots,N_y\}}$ and Z represents $(Z_k)_{k\in\{1,\ldots,N_y\}}$.

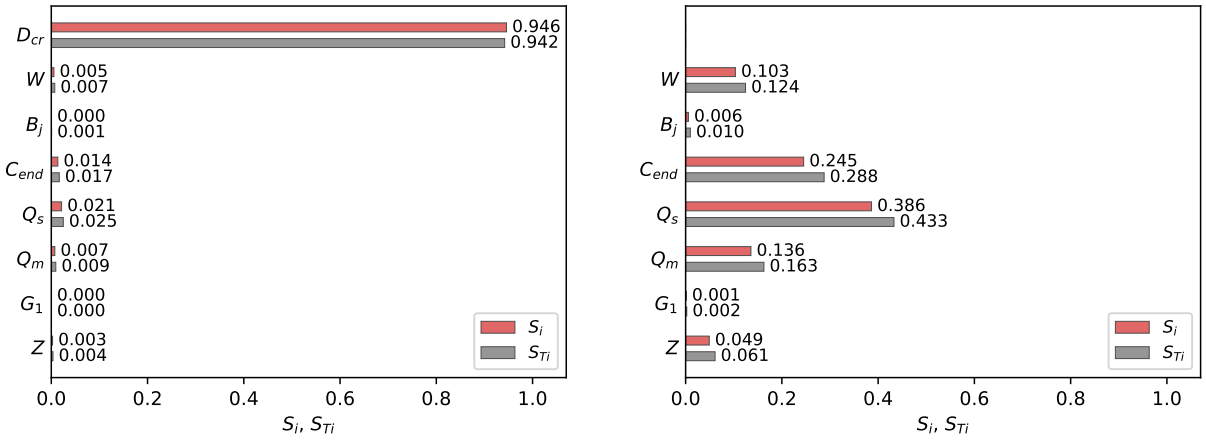

(a) Limit state function, $g(\boldsymbol{X}; N_y = 15, N = 500)$.

(b) Fatigue damage, $D_W(\boldsymbol{X}; N_y = 15, N = 500)$.

Figure 8: Sobol' indices for limit state function and weakest link fatigue damage for final year of base case. See Table 3 for a description of the variables.

Consider now the sensitivity indices for fatigue damage in Figure 8b. Firstly – and most importantly – the total effect indices are close to zero for B_j and for G_1. This means that the inferential uncertainty of the S-N curve coefficients and the annual variability of the representative mean loads are practically non-influential. Further implications are that (i) the simplification introduced by neglecting possible correlation between annual fatigue loads (Z) and mean loads (G^*_1) is justified, and (ii) (B_0, B_1, B_2) and G^*_1 may be fixed to their respective mean values for the subsequent reliability analysis with negligible impact on the estimated failure probability. Secondly, the sum of the first-order indices is $\sum_i S_i = 0.927$, meaning that roughly 7% of the fatigue damage uncertainty is caused by non-additive interaction effects. Judging by the difference between S_{Ti} and S_i, the variables with the most interaction are Q_s and C_{end} (although, not necessarily just with each other), followed by Q_m and W. Thirdly, the importance of modeling the annual variability of the fatigue loads (Z) is seen to be limited but not negligible, contributing to around 6% of the fatigue damage uncertainty in total.

The influence of the annual fatigue loads is investigated in more detail by assessing sensitivity indices for the fatigue load during each year, shown in Figure 9. Both the first-order and the total effect indices for Z_k increase with increasing k, meaning that the fatigue loads experienced during the last years influence the fatigue damage uncertainty more than those experienced during early years. The reason is the following. The expected corrosion grade increases with time, causing a temporal degradation of the expected fatigue

capacity. Uncertainty in annual fatigue load for the last years will therefore yield larger contributions to fatigue damage variance than uncertainty in fatigue loads for the first years. This effect causes the increase in the first-order index, S_i. The relatively larger increase in the total effect index (S_{Ti}) is because the corrosion grade uncertainty also increases with time, interacting with the fatigue load uncertainty in the final years.

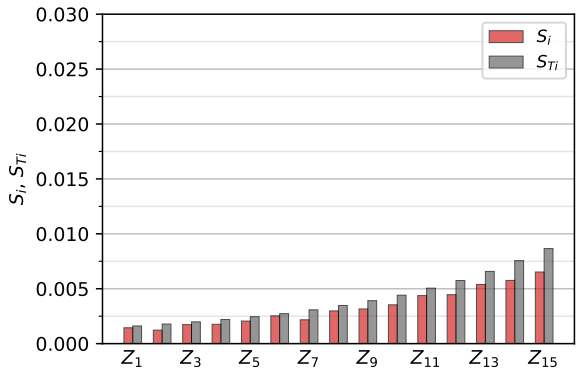

Figure 9: Sobol' indices for effect on $D_W(\boldsymbol{X}; N_y = 15, N = 500)$ from annual fatigue load uncertainty. Note the scale of the vertical axis.

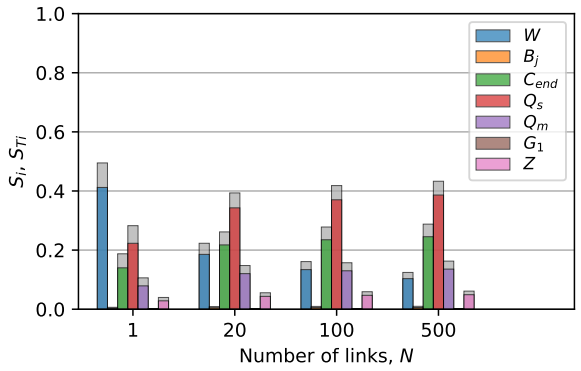

Figure 10: Sobol' indices for $D_W(\boldsymbol{X}; N_y = 15, N)$ with different segment sizes, N. First-order indices in foreground (color code in legend), and total effect indices in background (grey).

For the base case in Figure 8b, the uncertainty in weakest link resistance (W) is seen to be of moderate importance. Figure 10 shows how the Sobol' indices vary as a function of the segment size. For a single link ($N = 1$), the resistance is clearly the most influential variable. Its impact on the fatigue damage uncertainty drops quickly when the number of links is increased, and the dominant position is overtaken by the stress range uncertainty (Q_s), with larger impact also from the uncertainties in C_{end} and Q_m. This effect is consistent with a narrower distribution for W with increasing N, as previously illustrated in Example 5.

Keep in mind, however, that the reduced uncertainty for W will also result in less total variance for the fatigue damage. Since the sensitivity indices are normalized quantities, this is not reflected in Figure 10.

4.4.2. Reliability analysis

Based on the global sensitivity analysis, the S-N curve coefficients (B_0, B_1, B_2) and the annual mean loads G_1^* are now fixed to their mean values. This reduces the dimension of the model to $M = 5 + N_y$, that is, $M = 20$ random variables to calculate the failure probability after $N_y = 15$ years. Furthermore, the remaining random variables may be assumed to be mutually independent.

Resulting failure probabilities for the final year of the base case are shown in Table 4. The probability of failure estimated from importance sampling is based on a sample size of $N_{\mathrm{MC}} = 10^4$, which is seen to yield low uncertainty in the estimated value with a CoV of just 2%. It is also noted that FORM is seen to perform reasonably well for the current problem, with $p_{f,\mathrm{FORM}}/\hat{p}_{f,\mathrm{IS}} \approx 0.8$, indicating that the limit state surface is not too nonlinear in the vicinity of the design point.

Accumulated and annual failure probabilities differ by a factor of around 1.7 for the final year, with the annual failure probability on the low side. The temporal development of both quantities is compared in Figure 11, showing that the difference occurs mainly towards the end of the service life as the accumulated failure probability increases less steeply. In any case, the limited ratio between these quantities suggests that the use of either one over the other is unlikely to be decisive for the problem at hand.

Table 4: Results for the failure probabilities. Base case, final year ($N_y = 15$).

	Accumulated	Annual
β	3.63	
$p_{f,\mathrm{FORM}}$	1.42×10^{-4}	8.55×10^{-5}
$\hat{p}_{f,\mathrm{IS}}$	1.86×10^{-4}	1.08×10^{-4}
$\mathrm{CoV}(\hat{p}_{f,\mathrm{IS}})$	0.02	

The FORM design point is listed in Table 5, and the corresponding importance factors are visualized in Figure 12. Fatigue damage at failure (D_{cr}) is seen to be the most important variable. Nevertheless, its relative importance is far less than that suggested by the Sobol' indices for the limit state function (Figure 8a). A plausible explanation is the following. The lognormal distribution applied for D_{cr} is right-skewed. Since the Sobol' indices consider the uncertainty over the range of outcomes, they include the contribution from the upper (right) tail, which is fatter than the left tail. The design point, however, is located in the thinner left tail of the distribution, effectively reducing the importance of uncertainty in D_{cr} in the vicinity of the design point.

A striking observation from the importance factors for the current case (Figure 12) is that the model uncertainties (D_{cr}, Q_s and Q_m), that are quite likely the three most difficult variables to model accurately,

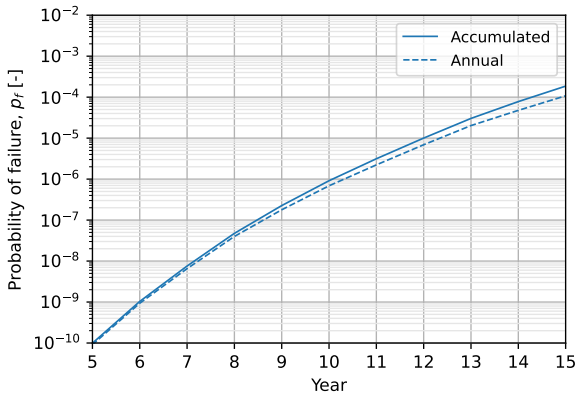

Figure 11: Probability of failure for the last 10 years of the base case, estimated by importance sampling. Comparison of accumulated vs. annual failure probabilities.

contribute to around 70% of the variance of the linearized limit state function. This stresses the potential benefit from improved modeling accuracy, or conversely, the potential pitfall in underestimating their uncertainties.

The relative importance of the corrosion grade uncertainty, expressed through C_{end}, is also reduced compared to that seen from the global sensitivity analysis (that is, relative to the other variables except D_{cr}). This may be explained by considering a 2–dimensional section through the design point and the failure surface ($g_{\boldsymbol{U}}(\boldsymbol{u}) = 0$) in standard normal space, shown in Figure 13. The distance from the failure surface to the origin of the U-space increases rapidly with increasing value for $U_3 = T_3(C_{\text{end}})$, meaning that no substantial contribution to the failure probability is obtained from going further into the tail of the distribution of C_{end}. This effect is a consequence of the corrosion grade scale applied. For the present work it is defined with an absolute upper limit of $c = 7$, as reflected by the uniform distribution used to model its uncertainty. Any degradation of the chain larger than that prescribed by $c = 7$ is thus precluded. Hence, it might be in its place to consider the need for a probability distribution that allows the corrosion grade to exceed 7, however small the probability.

Lastly, the importance of annual fatigue load variability is seen to be limited, with the sum of the importance factors for Z_k at only 4.3%. From Equation (68), the corresponding omission sensitivity factor is 1.02 if the fatigue load in each year is fixed to its expected value. For the reliability index given in Table 4, this implies that the (FORM) failure probability is underestimated by a factor of $\Phi(-\beta)/\Phi(-\beta \cdot 1.02) \approx 1.3$ if the annual fatigue load variability is neglected, an error that may be considered negligible in this context. Even so, we will retain the fatigue load variability for the subsequent parameter variation so that the influence on failure probability in earlier years may be assessed.

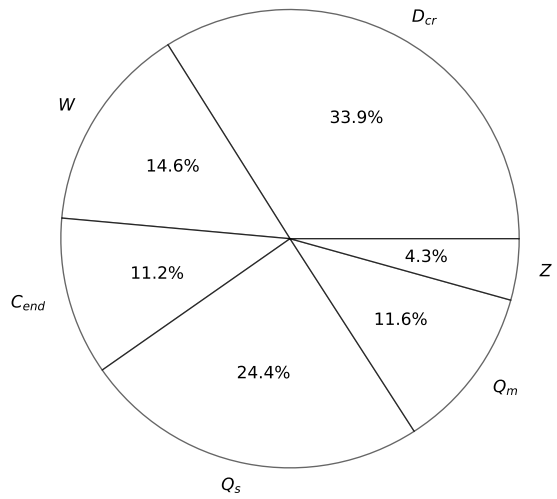

Figure 12: FORM importance factors, α_i^2. Importance factor for Z is the sum of α_i^2 for $(Z_k)_{k\in\{1,\dots,N_y\}}$.

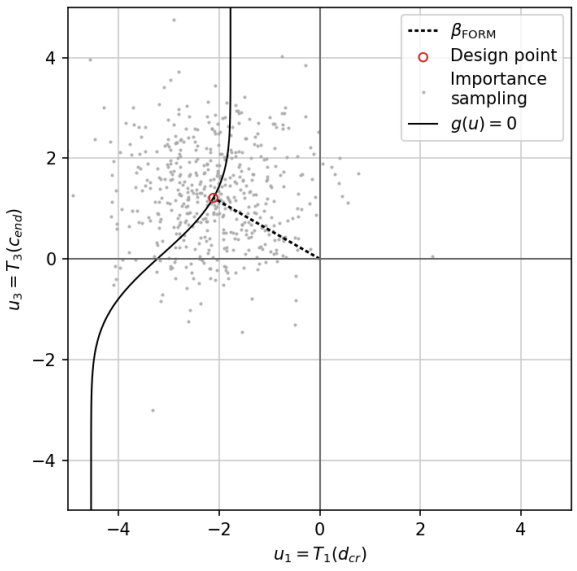

Figure 13: FORM design point in standard normal space for C_{end} and D_{cr}, along with a section of the failure surface and 500 points from the importance sampling.

Table 5: FORM design point for base case, final year ($N_y = 15$). Data for $Z_2 - Z_{14}$ lie in the range between the values listed for Z_1 and Z_{15}, and are omitted here.

X_i	u_i^*	x_i^*	$F_{X_i}(x_i^*)$
D_{cr}	-2.11	0.53	0.017
W	-1.39	0.25	0.083
C_{end}	1.21	6.32	0.89
Q_s	1.79	1.18	0.96
Q_m	1.23	1.12	0.89
Z_1	0.09	4.80×10^8	0.54
Z_{15}	0.32	5.26×10^8	0.63

4.4.3. Parametric study

The effect on probability of fatigue failure from selected parameters is now assessed. The parameters that are varied may be grouped roughly into two main categories: (i) those that may be regarded as system properties (annual fatigue load, representative mean load, number of chain links), and (ii) modeling parameters or choices (corrosion parameters, S-N model with or without mean load and corrosion dependency). Results for the last ten years of the service life are presented in Figure 14, in terms of annual failure probability obtained from importance sampling with sample size $N_{\text{MC}} = 10^4$. Each of the cases is described and discussed in the following paragraphs.

Annual fatigue load variability. The CoV of the annual fatigue load is varied in Figure 14a, from the base case with $\text{CoV}(Z) = 0.40$ and down to a lowest value of $\text{CoV}(Z) = 0.05$. For the final year, the difference in failure probability is less than a factor of 1.3. This is consistent with the omission sensitivity factor discussed previously, predicting a negligible error for failure probability after 15 years if the variability of Z is neglected. A larger difference is observed for the first years shown in the figure (i.e., years 5-6), but the ratio between the failure probabilities for largest and lowest fatigue load variability is still within one order of magnitude.

Mean annual fatigue load. In Figure 14b, the expected annual fatigue load is varied by $\pm 20\%$ and $\pm\, 40\%$ compared to the base case value. With stress range effect $m = 3$, this corresponds to adjustments of the nominal chain diameter ranging from -5% to $+10\%$ (for highest and lowest fatigue loads, respectively) – if one assumes that the tension range distribution is unaffected by the change in diameter.[10] The expected fatigue damage is directly proportional the to mean annual fatigue load (cf. Equation (27)), and thus increases by the same factor as $\text{E}[Z]$. This has a substantial effect on the failure probability, as one might

[10] In practice, a change in chain diameter will also affect the mean load measured in percentage of MBL, and thereby affect the failure probability also through a reduction or increase in fatigue capacity.

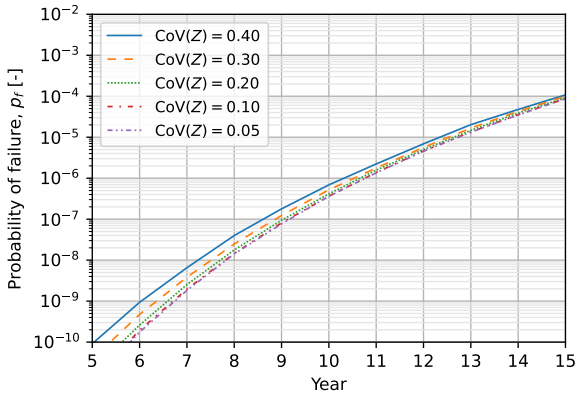

(a) CoV of annual fatigue load.

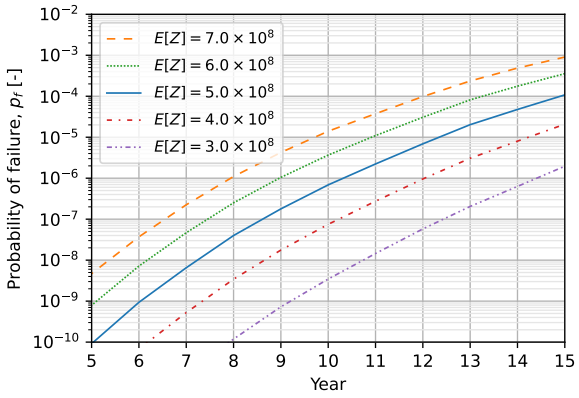

(b) Mean annual fatigue load.

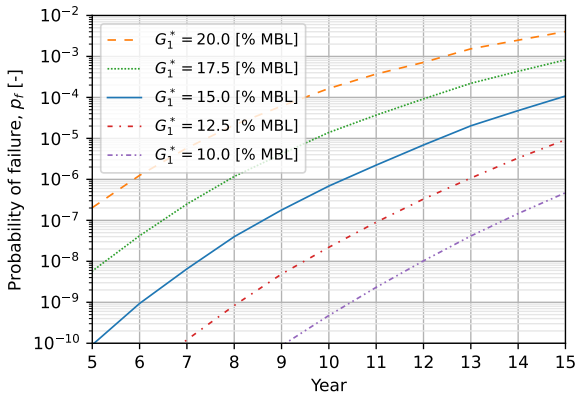

(c) Representative mean load.

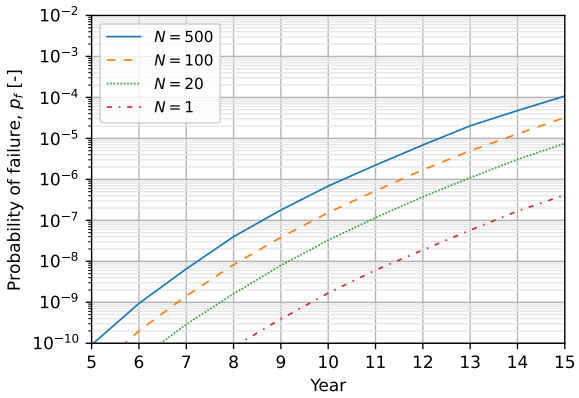

(d) Number of links.

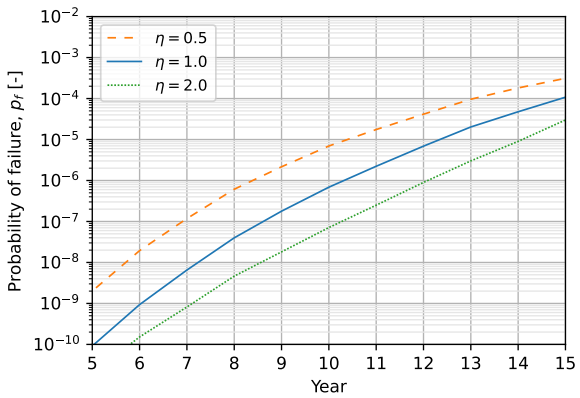

(e) Corrosion grade development.

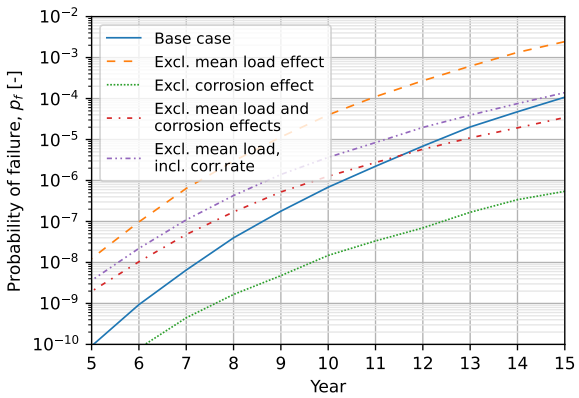

(f) Treatment of mean load and corrosion effects.

Figure 14: Parametric study: influence of fatigue load, mean load, number of links, corrosion grade development and treatment of mean load and corrosion effects on probability of failure. Bases case result is shown by solid blue line in all subfigures. See main text for case descriptions.

expect. An increase of E[Z] by 40% increases the probability of failure by one order of magnitude for the final year, whereas a reduction of E[Z] by 40% reduces it by nearly two orders of magnitude.

Representative mean load. The effect of the representative mean load is shown in Figure 14c, for mean loads ranging from 10% to 20% of MBL – all of which are realistic mean load levels for offshore mooring systems. The mean load effect on the fatigue capacity is seen to significantly impact the fatigue reliability. Compared to the base case at 15% MBL, a change in mean load by ±2.5% MBL increases or reduces the failure probability by approximately one order of magnitude. For 10% mean load the failure probability is more than two orders of magnitude below the base case, whereas for 20% it is higher by a factor of 40.

Number of links. In Figure 14d, the segment size is varied between $N = 1$ (single link) and $N = 500$. The resulting weakest link distributions are identical to those presented in Example 5. The probability of failure for the last year with $N = 500$ is larger by a factor of roughly 10 compared to the much shorter segment with $N = 20$, and larger by more than two orders of magnitude compared to $N = 1$. This leads to the following interesting observation. If we consider the simplified treatment of dependence between links described in Example 3, the upper bound of the segment failure is $p_f^{(N)} \leq 1 - (1 - p_f^{(1)})^N$ (corresponding to independent failure events for each of the links, see Equation (9)). From Figure 14d we obtain $p_f^{(1)} = 4{\times}10^{-7}$, which gives the upper bound $p_f^{(500)} \leq 2 \times 10^{-4}$. Compared to the value obtained here, $p_f^{(500)} \approx 1 \times 10^{-4}$, the upper bound is larger by a factor of 2 (which is quite modest in connection with failure probabilities, for which orders of magnitude are most important). This means that the current reliability formulation yields results that correspond closely to independent failure events. In other words; *the assumption that ϵ_i is independent between links has, in practice, a much stronger effect on the failure probability than the assumption of variables that are fully dependent between links* (i.e., $D_{\text{cr}}, Z, C_{\text{end}}, Q_s$ and Q_m among those that have not been fixed).

Corrosion grade development. We now consider variation of the corrosion grade development in Figure 14e. The legend descriptions refer to the shape parameter in Equation (7) (see also Figure 4). With $\eta = 0.5$, the corrosion grade is assumed to develop more rapidly towards its value at the end of the service life. For early years, this is seen to increase the failure probability by more than one order of magnitude compared to the base case with $\eta = 1$. In the final year, however, the difference is reduced to a factor of around 3. If a slower initial corrosion grade development is assumed ($\eta = 2$), accelerating towards the end of the service life, the failure probability in the final year is a factor of 3 below the base case. Hence, for the two very different corrosion grade histories described by $\eta = 0.5$ and $\eta = 2$, the difference in failure probability is around one order of magnitude at the end of the service life.

Treatment of mean load and corrosion effects. The cases considered in Figure 14f require some further explanations. Referring to the figure legend, these are defined as follows:

1) *Excl. mean load effect*: Mean load effect on fatigue capacity is neglected, i.e., fixed values $G_1^* = 20$ [% MBL] and $Q_m = 1$ are used.
2) *Excl. corrosion effect*: Degradation due to corrosion is neglected, by fixing $C_{\text{end}} = 1$.
3) *Excl. mean load and corrosion effects*: The first two cases combined.
4) *Excl. mean load, incl. corr. rate*: Same as the previous case, but corrosion is accounted for by a reduction of the cross section area, expressed though a corrosion rate describing the annual material loss. See Appendix A for related calculations. We have assumed that the nominal diameter is 120 mm, and a (fixed) corrosion rate of 0.4 mm/year is applied.

Note that the latter case resembles how corrosion is accounted for in the current design code approach [2]. The results in Figure 14f show that the failure probability is significantly overestimated if one neglects the mean load effect while at the same time accounting for degradation due to corrosion (case 1). Conversely, the failure probability is underestimated by even more if the beneficial effect of a mean load below 20% is realized without accounting for corrosion (case 2). When both mean load and degradation are neglected (case 3), the failure probability increases less steeply with time. Compared to the base case, it is overestimated for the early years and underestimated for the final years. A similar development of the failure probability with time is seen for the case with a simplified corrosion model (case 4), slightly on the high side of the previous case. Coincidentally, the failure probability in the final year matches that obtained for the base case. However; (i) the good agreement would not be seen if a different mean load had been applied for the base case, and (ii) the failure probability in subsequent years would most likely be underestimated by the simplified approach, considering the different slopes of the curves.

4.5. Conclusions of case study

A global sensitivity analysis was used to identify non-influential variables and to assess the amount of interactions in the model. For the applied S-N model and the case defined for the present study it was found that (i) the S-N curve coefficients (B_0, B_1, B_2) and the annual representative mean load (G_1^*) may be fixed to their mean values with negligible impact on the fatigue damage variance, and (ii) the random variables interact moderately within the model, with interactions contributing around 7% of the uncertainty in fatigue damage after 15 years for the base case.

A reliability analysis was conducted thereafter, including variation of system properties and model parameters. The main findings were the following:

- Based on the FORM importance factors, fatigue failure is dominated by the model uncertainties (uncertainty in Miner's rule, as well as stress range and mean load uncertainties).
- The relative importance of uncertainty in corrosion grade is constrained by the choice of a uniform distribution to represent it, thereby restricting the maximum degradation of the chain.

- Annual fatigue load variability has insignificant influence on the failure probability, expect for the early years of service, despite temporal degradation of the fatigue capacity and some degree of interaction with the corrosion grade uncertainty.
- The formulation for *segment* failure gives results that are close to those obtained if independent events with equal probability are assumed for failure of individual links. This indicates that the assumption of independent S-N model regression errors has a stronger effect on the reliability than the assumptions that all the links are exposed to the same loads and degradation, and that they fail at the same critical level of fatigue damage.
- Mean load and degradation due to corrosion both have a substantial impact on the failure probability. These effects have, in practice, opposite consequences for fatigue life. *Coincidentally*, for the particular case considered here, including both effects leads to similar failure probability at end of service life as neglecting both. This is not true in general.
- Accounting for corrosion in a simplified way, through a corrosion rate describing the annual reduction of the chain diameter (and a corresponding increase in fatigue load), considerably underestimates the corrosion effect on fatigue reliability compared to that predicted by the S-N model used for the present study.

5. Conclusions

A new reliability formulation for fatigue failure of mooring chain segments has been developed, accounting for the effects on fatigue capacity from mean load and degradation due to corrosion. The limit states function is defined from a summation of the fatigue damage contribution per year of service, which enables accounting for (i) both known fatigue loads during prior years of service and future, uncertain loads, and (ii) the temporal development of the corrosion condition of the chain.

Partial dependence between the failure events of individual links within a segment is handled by distinguishing between variables that are either independent between links or fully dependent and take on the same values. This leads to a weakest link formulation, making it straightforward to assess the fatigue reliability for arbitrary segment size.

A thorough case study of a realistic floating system has been presented. We demonstrated the effect on fatigue failure probability from a range of parameters, including system properties and modeling assumptions. Specifically, it was found that the mean load and corrosion effects strongly influence the fatigue reliability of mooring chain, and must *both* be accounted for to avoid the risk of considerably over- or underestimating the failure probability. The case study results thus support the need for a fatigue reliability formulation that accounts properly for mean load and chain degradation.

Acknowledgment

This study was financed by the Research Council of Norway, through the project 280705 "Improved lifetime estimation of mooring chains" (LIFEMOOR).

Appendix A. Design code calculations

Appendix A.1. Maximum allowable annual fatigue load

The design equation for the fatigue limit state is [2]

$$d_c \cdot \gamma_F \leq 1 \tag{A.1}$$

where d_c is a characteristic fatigue damage and γ_F is the fatigue safety factor. Let L denote the service life in years, and let $d_{c,\mathrm{yr}}$ denote the average, characteristic fatigue damage per year. The design equation may then be written

$$L \cdot d_{c,\mathrm{yr}} \cdot \gamma_F \leq 1 \tag{A.2}$$

Now, the average annual fatigue damage may be expressed as

$$d_{c,\mathrm{yr}} = \frac{\mathrm{E}[n_0 \cdot S^m]}{A_D} = \frac{\overline{Z}}{A_D} \tag{A.3}$$

where A_D is the intercept parameter of the S-N design curve and $\overline{Z} = \mathrm{E}[Z]$ is the expected annual fatigue load. Combining (A.2) and (A.3), the maximum allowable annual fatigue load becomes

$$\overline{Z} \leq \frac{A_D}{L \cdot \gamma_F} \tag{A.4}$$

Hence, with $L = 15$ [years], $\gamma_F = 8$ and $A_D = 6 \times 10^{10}$ [2], we get $\bar{Z} \leq 5 \times 10^8$ [MPa^3].

Appendix A.2. Correction for material loss

When corrosion is accounted for by means of a corrosion rate, representing the annual material loss, the effective chain diameter after k years is

$$\mathrm{d}_\mathrm{k}^{(\mathrm{crs})} = \mathrm{d}_0^{(\mathrm{crs})} - c_r \cdot k \tag{A.5}$$

where $\mathrm{d}_0^{(\mathrm{crs})}$ is the nominal diameter and c_r is the corrosion rate expressing the reduction in diameter per year. For a given tension range distribution, the annual fatigue load is inversely proportional to the cross section area raised to m (the S-N curve stress range effect). The expected fatigue load in the k^{th} year is therefore related to the effective diameter by

$$\overline{Z}_k \propto \left(\frac{1}{\mathrm{d}_\mathrm{k}^{(\mathrm{crs})}} \right)^{2m} \tag{A.6}$$

Combining (A.5) and (A.6), a scaling factor for the expected effective fatigue load may thus be expressed as

$$\frac{\bar{Z}_k}{\bar{Z}_0} = \left(1 - \frac{c_r \cdot k}{\mathrm{d}_0^{(\mathrm{crs})}}\right)^{-2m} \tag{A.7}$$

where $\bar{Z}_0$ is the expected annual fatigue load calculated based on the nominal diameter.

Nomenclature

X_i	i^{th} component of random vector $\boldsymbol{X}$
E[.]	Mathematical expectation
P[.]	Probability measure
Var[.]	Variance
ln(.)	Natural logarithm
log(.)	Common logarithm
$\sim$	distributed as
$LN(\mu, \sigma)$	Lognormal distribution with scale parameter $\exp\{\mu\}$ and shape parameter σ
$N(\mu, \sigma^2)$	Normal distribution with mean μ and variance σ^2
$U(a, b)$	Uniform distribution with support $[a, b]$
$\mathbb{N}^*$	Natural integers excluding 0, i.e., $\{1, 2, 3, \ldots\}$
$\mathbb{N}^*_M$	Natural integers less than M excluding 0, i.e., $\{1, 2, \ldots, M\}$
$\mathbb{R}_+$	Real numbers greater than or equal to zero
α_i	FORM importance factor, for $i \in \mathbb{N}^*_M$, see (66)
β	FORM reliability index, see (57)
ϵ	Regression error, see (3)
η	Exponent of probabilistic corrosion model, see (7)
μ	Logarithm of scale parameter of lognormal distribution Mean value

σ	Shape parameter of lognormal distribution Standard deviation
σ_m	Mean stress [MPa]
$A(\sigma_m, c)$	Mean load and corrosion dependent intercept parameter of S-N curve, see (2)
B_0	Coefficient of S-N curve intercept parameter, see (2)
B_1	Coefficient of S-N curve intercept parameter (mean load effect), see (2)
B_2	Coefficient of S-N curve intercept parameter (corrosion grade effect), see (2)
c	Corrosion grade, support $[1, 7]$
C_{end}	Corrosion grade at end of service life, see (7)
D	Fatigue damage (Palmgren-Miner sum)
D_W	Fatigue damage of weakest link in a segment, see (21)
D_{cr}	Critical fatigue damage, i.e., Miner's sum at failure
$g(\boldsymbol{X}; N_y, N)$	Limit state function for fatigue failure after N_y years for chain segment with N links
$g_1(\sigma_m)$	Mean load function, see (2)
G_1^*	Representative value of mean load function over a specified period, see (6)
$g_2(c)$	Corrosion grade function, see (2)
G_2^*	Representative value of corrosion grade function over a specified period
$g_{\boldsymbol{U}}(\boldsymbol{U})$	Limit state function in standard normal space, see (55)
k	Index for year, for $k \in \{1, 2, \ldots, N_y\}$
M	Dimension of random vector
m	Slope parameter of S-N curve
N	Number of cycles to failure, see (1) Number of links in the chain segment, see (17) and
N_y	Number of years
N_{MC}	Sample size (number of realizations) generated in Monte Carlo simulation

$p_f^{(N)}$	Probability of failure for segment with N links, see (22)
Q_s, Q_m, Q_c	Model uncertainties for stress ranges, mean loads and corrosion grade, respectively, see Section 3.3
S	Stress range [MPa]
S_i	First-order Sobol' index, for $i \in \mathbb{N}_M^*$, *see*(47)
S_{Ti}	Total effect Sobol' index, for $i \in \mathbb{N}_M^*$, *see*(48)
W	Deviation from median fatigue capacity for weakest link in a segment, see (17)
Z	Fatigue load, see (4)
CoV	Coefficient of Variation
FORM	First Order Reliability Method
i.i.d.	independent and identically distributed
IS	Importance Sampling
MBL	Minimum Breaking Load
MCS	Monte Carlo Simulation

References

[1] ISO 19901-7, Petroleum and natural gas industries - Specific requirements for offshore structures - Part 7: Stationkeeping systems for floating offshore structures and mobile offshore units (2013).

[2] DNV GL, Offshore Standard - Position mooring (DNVGL-OS-E301), Edition July 2018 (2018).

[3] J. Mathisen, T. Hørte, V. Moe, W. Lian, Joint Industry Project – DEEPMOOR – Design Methods for Deep water Mooring Systems, Calibration of a Fatigue Limit States, DNV Report 97-3583, Rev. 03, Det Norske Veritas (1999).

[4] J. Mathisen, T. Hørte, Calibration of a Fatigue Limit State for Mooring Lines, in: International Conference on Computational Methods in Marine Engineering MARINE 2005, Barcelona, 2005.

[5] K.-t. Ma, H. Shu, P. Smedley, D. L'Hostis, A. Duggal, A Historical Review on Integrity Issues of Permanent Mooring Systems, in: Offshore Technology Conference, no. OTS-24025-MS, Offshore Technology Conference, Houston, Texas, USA, 2013. doi:10.4043/24025-MS.
URL https://doi.org/10.4043/24025-MS

[6] A. Kvitrud, Lessons Learned From Norwegian Mooring Line Failures 2010–2013, in: Proceedings of the ASME 2014 33rd International Conference on Ocean, Offshore and Arctic Engineering, 2014, pp. 1–10. doi:10.1115/OMAE2014-23095.

[7] E. Fontaine, A. Kilner, C. Carra, D. Washington, K. T. Ma, A. Phadke, D. Laskowski, G. Kusinski, Industry Survey of Past Failures, Pre-emptive Replacements and Reported Degradations for Mooring Systems of Floating Production Units, in: Offshore Technology Conference, no. OTC-25273-MS, Offshore Technology Conference, Houston, Texas, 2014. doi:10.4043/25273-MS.
URL https://doi.org/10.4043/25273-MS

[8] Ø. Gabrielsen, K. Larsen, O. Dalane, H. B. Lie, S.-A. Reinholdtsen, Mean Load Impact on Mooring Chain Fatigue Capacity: Lessons Learned From Full Scale Fatigue Testing of Used Chains, in: Proceedings of the ASME 2019 38th International Conference on Ocean, Offshore and Arctic Engineering, no. OMAE2019-95083, 2019. doi:https://doi.org/10.1115/OMAE2019-95083.

[9] J. Fernández, A. Arredondo, W. Storesund, J. J. González, Influence of the Mean Load on the Fatigue Performance of Mooring Chains, in: Proceedings of the Annual Offshore Technology Conference, no. OTC-29621-MS, 2019. doi:10.4043/29621-MS.

[10] Y. Zhang, P. Smedley, Fatigue Performance of High Strength and Large Diameter Mooring Chain in Seawater, in: Proceedings of the ASME 2019 38th International Conference on Ocean, Offshore and Arctic Engineering, no. OMAE2019-95984, 2019. doi:https://doi.org/10.1115/OMAE2019-95984.

[11] K.-t. Ma, Ø. Gabrielsen, Z. Li, D. Baker, A. Yao, P. Vargas, M. Luo, A. Izadparast, A. Arredondo, L. Zhu, N. Sverdlova, I. S. Høgsæt, Fatigue Tests on Corroded Mooring Chains Retrieved From Various Fields in Offshore West Africa and the North Sea, in: Proceedings of the ASME 2019 38th International Conference on Ocean, Offshore and Arctic Engineering, no. OMAE2019-95618, 2019.

[12] E. N. Lone, T. Sauder, K. Larsen, B. J. Leira, Fatigue assessment of mooring chain considering the effects of mean load and corrosion, in: Proceedings of the ASME 2021 40th International Conference on Ocean, Offshore and Arctic Engineering, no. OMAE2021-62775, Virtual, 2021. doi:10.1115/OMAE2021-62775.

[13] E. N. Lone, T. Sauder, K. Larsen, B. J. Leira, Probabilistic fatigue model for design and life extension of mooring chains, including mean load and corrosion effects, Ocean Engineering 245 (2022) 110396. doi:10.1016/j.oceaneng.2021.110396.
URL https://linkinghub.elsevier.com/retrieve/pii/S0029801821016863

[14] A. Gelman, J. Hill, Data Analysis Using Regression and Multilevel/Hierarchical Models, Analytical methods for social research, Cambridge University Press, Cambridge, 2007. doi:10.1017/CBO9780511790942.

[15] P. H. Wirsching, Fatigue Reliability for Offshore Structures, Journal of Structural Engineering 110 (10) (1984) 2340–2356. doi:10.1061/(ASCE)0733-9445(1984)110:10(2340).

[16] P. Thoft-Christensen, Y. Murotsu, Application of Structural Systems Reliability Theory (1986).

[17] K. Larsen, J. Mathisen, Reliability-based fatigue analysis of mooring lines, in: Proceedings of the 15th International Conference on Ocean, Offshore Mechanics and Arctic Engineering, 1996.

[18] I. Lotsberg, Fatigue Design of Marine Structures, Cambrige University Press, 2016. doi:https://doi.org/10.1017/CBO9781316343982.

[19] K. Bury, Statistical Distributions in Engineering, Cambridge University Press, 1999. doi:10.1017/CBO9781139175081.
URL https://www.cambridge.org/core/product/identifier/9781139175081/type/book

[20] M. Lemaire, Structural Reliability, ISTE, London, UK, 2009. doi:10.1002/9780470611708.
URL http://doi.wiley.com/10.1002/9780470611708

[21] V. Aksnes, P. A. Berthelsen, N. M. M. D. D. Fonseca, S.-A. Reinholdtsen, On the Need for Calibration of Numerical Models of Large Floating Units against Experimental Data, in: Proceedings of the Twenty-fifth International Ocean and Polar Engineering Conference, International Society of Offshore and Polar Engineers, 2015.
URL http://onepetro.org/ISOPEIOPEC/proceedings-pdf/ISOPE15/All-ISOPE15/ISOPE-I-15-264/1342795/isope-i-15-264.pdf/1

[22] T. Sauder, Empirical estimation of low-frequency nonlinear hydrodynamic loads on moored structures, Applied Ocean Research 117 (2021) 102895. doi:10.1016/J.APOR.2021.102895.
URL https://linkinghub.elsevier.com/retrieve/pii/S0141118721003667

[23] T. Sauder, P. Mainçon, E. Lone, B. J. Leira, Estimation of top tensions in mooring lines by sensor fusion, Preprint submitted to Marine Structures (2022).

[24] Ø. Gabrielsen, S.-A. Reinholdtsen, B. Skallerud, P. J. Haagensen, M. Andersen, P.-A. Kane, Fatigue Capacity of Used Mooring Chain - Results from Full Scale Fatigue Testing at Different Mean Loads, in: Proceedings of the ASME 2022 41st International Conference on Ocean, Offshore and Arctic Engineering, no. OMAE2022-79649, Hamburg, Germany, 2022.

[25] R. Melchers, A. T. Beck, Structural reliability analysis and prediction, 3rd Edition, John Wiley & Sons, Inc., Hoboken, NJ, 2018.

[26] K. Bury, Distribution of smallest log-normal and gamma extremes, Statistische Hefte 16 (2) (1975) 105–114. doi:10.1007/BF02922919.
URL http://link.springer.com/10.1007/BF02922919

[27] P. H. Wirsching, Y. N. Chen, Considerations of Probability-Based Fatigue Design for Marine Structures, Marine Structures 1 (1) (1988) 23–45. doi:10.1016/0951-8339(88)90009-3.

[28] JCSS, Probabilistic Model Code. Part 3: Resistance Models. Section 3.12 Fatigue, Joint Committee on Structural Safety, 2011.

[29] J. N. Kapur, Maximum-entropy Models in Science and Engineering, John Wiley & Sons, New York, 1989.

[30] I. Sobol', Sensitivity estimates for nonlinear mathematical models, Math. Model. Comput. Exp. 1 (4) (1993) 407–414.

[31] A. Saltelli, M. Ratto, T. Andres, F. Campolongo, J. Cariboni, D. Gatelli, M. Saisana, S. Tarantola, Global Sensitivity Analysis. The Primer, John Wiley & Sons, Ltd, Chichester, UK, 2008. doi:10.1002/9780470725184.
URL http://doi.wiley.com/10.1002/9780470725184

[32] J. Jacques, C. Lavergne, N. Devictor, Sensitivity analysis in presence of model uncertainty and correlated inputs, Reliability Engineering & System Safety 91 (10-11) (2006) 1126–1134. doi:10.1016/j.ress.2005.11.047.
URL https://linkinghub.elsevier.com/retrieve/pii/S0951832005002231

[33] A. Saltelli, P. Annoni, I. Azzini, F. Campolongo, M. Ratto, S. Tarantola, Variance based sensitivity analysis of model output. Design and estimator for the total sensitivity index, Computer Physics Communications 181 (2) (2010) 259–270. doi:10.1016/j.cpc.2009.09.018.
URL https://linkinghub.elsevier.com/retrieve/pii/S0010465509003087

[34] B. Sudret, Global sensitivity analysis using polynomial chaos expansions, Reliability Engineering and System Safety 93 (7) (2008) 964–979. doi:10.1016/j.ress.2007.04.002.

[35] R. Rackwitz, B. Fiessler, Structural reliability under combined random load sequences, Computers & Structures 9 (5) (1978) 489–494. doi:10.1016/0045-7949(78)90046-9.
URL https://linkinghub.elsevier.com/retrieve/pii/0045794978900469

[36] Y. Zhang, A. Der Kiureghian, Two Improved Algorithms for Reliability Analysis, in: R. Rackwitz, G. Augusti, A. Borri (Eds.), Reliability and Optimization of Structural Systems, Springer US, Boston, MA, 1995, pp. 297–304. doi:10.1007/978-0-387-34866-7_32.
URL https://link.springer.com/chapter/10.1007/978-0-387-34866-7{_}32http://link.springer.com/10.1007/978-0-387-34866-7{_}32

[37] P. Virtanen, R. Gommers, T. E. Oliphant, M. Haberland, T. Reddy, D. Cournapeau, E. Burovski, P. Peterson, W. Weckesser, J. Bright, S. J. van der Walt, M. Brett, J. Wilson, K. J. Millman, N. Mayorov, A. R. J. Nelson, E. Jones, R. Kern, E. Larson, C. J. Carey, l. Polat, Y. Feng, E. W. Moore, J. VanderPlas, D. Laxalde, J. Perktold, R. Cimrman, I. Henriksen, E. A. Quintero, C. R. Harris, A. M. Archibald, A. H. Ribeiro, F. Pedregosa, P. van Mulbregt, SciPy 1.0: fundamental algorithms for scientific computing in Python, Nature Methods 17 (3) (2020) 261–272. doi:10.1038/s41592-019-0686-2.
URL https://doi.org/10.1038/s41592-019-0686-2http://www.nature.com/articles/s41592-019-0686-2

[38] H. O. Madsen, Omission sensitivity factors, Structural Safety 5 (1) (1988) 35–45. doi:10.1016/0167-4730(88)90004-5.

[39] I. Papaioannou, D. Straub, Variance-based reliability sensitivity analysis and the FORM α-factors, Reliability Engineering

& System Safety 210 (2021) 107496. doi:10.1016/j.ress.2021.107496.
URL https://doi.org/10.1016/j.ress.2021.107496https://linkinghub.elsevier.com/retrieve/pii/S0951832021000612

[40] D. Straub, R. Schneider, E. Bismut, H.-J. Kim, Reliability analysis of deteriorating structural systems, Structural Safety 82 (2020) 101877. doi:10.1016/j.strusafe.2019.101877.
URL https://linkinghub.elsevier.com/retrieve/pii/S0167473018303254